Reliability Assessment of Offshore Platforms in Seismic Regions

by

J. N. Yang, and A. M. Freudenthal

Technical Report No. 2

Sponsored by
The National Science Foundation
through Grant ENV-75-06895
August, 1977

School of Engineering and Applied Science
The George Washington University
Washington, D.C. 20052

TABLE OF CONTENTS

Acknowledgement

The authors would like to thank Dr. S. C. Liu of NSF for his interest and encouragement of this study. Some numerical computations carried out by the graduate student, Mr. M. D. Liu, is acknowledged.

I. Introduction

It is well-known that most of the environmental loadings (threats) to offshore platforms are statistical in nature. Because of the serious consequence of structural failure, the reliability analysis of the offshore platforms has attracted increasing attention recently [e.g., Refs. 1-4]. The reliability analysis technique used for the offshore platforms is essentially the application of the principles of classical structural reliability [e.g., Refs. 5-9] in conjuction with appropriate design criteria [e.g., Refs. 10-13]. Basically, two environmental threats are most important; (i) the storm waves (hurricanes), and (ii) the strong earthquakes. Extensive investigations have been made with regard to the storm waves [e.g., Refs. 14-23, 3] and the strong earthquakes [e.g., Refs. 24-29, 2] in application to the analysis and design of offshore platforms. In addition, almost all of the literature in the area of earthquake engineering [e.g., Refs. 30-35] is useful to the reliability analysis of offshore structures under strong earthquakes.

The investigation of the dynamic response of the structures to the above-mentioned environmental loadings is an important segment in the process of reliability analysis. Most of the literature available to-date [e.g., Refs. 36-43] uses the method of equivalent linearization [e.g., Refs. 44-45]. Furthermore, the failure modes and the associated resisting strengths of the offshore platforms have also been investigated [e.g., Refs. 1, 13, etc.].

It is the purpose of this paper to present a method of reliability analysis and design for the offshore platforms under stochastic dynamic loads during their design service life. The present approach combines the analyses of non-linear random vibration and the first passage probability [e.g., Refs. 36-40, 44, 46-48], and hence it is more accurate than the conventional equivalent static or quasi-static design procedures. The reliability design is then examined to establish the conditions under which the design for one loading condition (such as storm waves) is sufficient, as well as the conditions under which both the storm waves and the earthquakes are equally important.

The structure has to survive the stochastic storm waves, earthquakes, and the simultaneous occurrences of both during its design service life. The occurrences of the storm waves and the earthquakes are modeled as homogeneous Poisson processes, respectively. The simultaneous occurrence of both the storm waves and the earthquakes is shown to be another homogeneous Poisson process; the occurrence rate of which is a function of the occurrence rates and the average durations of both the storm waves and the earthquakes.

The applied loads due to storm waves and earthquakes, once they occur, are modeled as stationary Gaussian random processes with zero mean and finite duration. In this connection, the Pierson-Moskowitz wave height spectrum and an empirical ground acceleration spectrum have been used [e.g., Refs. 14, 30, 36-40]. The maximum wave height and the maximum ground motion (acceleration or velocity) vary from one storm and earthquake to another in the course of the design service life; hence

they are random variables. The statistical distributions of these random variables are available from past records at some potentially oil-rich sites, such as the Gulf of Alaska, the Gulf of Mexico, the North Sea, etc. This information has been used in the present analysis.

A nonlinear vibration analysis of the offshore structure under stochastic storm waves and earthquakes is carried out, following essentially the approach employed by Penzien et al [Refs. 36-40], to obtain the response statistics of the shear forces and the bending moments induced in the structure.

The resisting strength of the platform associated with each failure mode is a random variable assumed to follow the Weibull distribution. With all the information described above, a first passage failure analysis [e.g., Refs. 44, 46-48] is performed to estimate the probability of failure of the structure during its design service life.

It is shown that for deep water offshore platforms, the storm waves dominate the design criteria in the Gulf of Alaska, while the earthquake loadings and the joint occurrences of both the storm waves and the earthquakes are not important. The importance of the earthquake design relative to the storm wave design is expected to increase as the water depth decreases. It is further shown that the nonlinear drag force is extremely important in the design of deep offshore platforms and it must not be neglected.

II Reliability of Structures in Design Service Life

The offshore tower is considered to be subjected to three types of stochastic loadings (processes) in its design service life, (i) the storm waves $X_1(t)$, (ii) the earthquakes $X_2(t)$, and (iii) the simultaneous occurrences of both the storm waves and the earthquakes $X_3(t)$. Other types of loadings, such as current, tsunami, etc., will be discussed later. A schematic diagram for these loadings are displayed in Fig. 1.

Let $L_1(t)$, $L_2(t)$ and $L_3(t)$ be the reliabilities of the offshore tower in the service time interval (0,t), respectively, due to the storm waves, $X_1(t)$, the earthquakes, $X_2(t)$, and the simultaneous occurrence of both, $X_3(t)$. Then, with a reasonable assumption that the occurrence of the storm waves $X_1(t)$ is statistically independent of the occurrence of the earthquakes, $X_2(t)$, the reliability of the structure in the service time interval (0,t) is

$$L(t) \simeq L_1(t)\ L_2(t)\ L_3(t) \tag{1}$$

(i) Structural reliability $L_1(t)$ Under Storm Waves $X_1(t)$

The storm waves $X_1(t)$ is modeled as a homogeneous Poisson process with an average occurrence rate λ_1 per year (or return period $1/\lambda_1$ years). It is written mathematically as

$$X_1(t) = \sum_{i=1}^{N_1} A_{1i}(t)\left[H\left(t-t_{1i}\right) - H\left(t-t_{1i}-T_{1i}\right)\right] \tag{2}$$

in which H() is the unit step function, $A_{1i}(t)$ is the wave height process of the ith storm occurring at t_{1i} with a duration T_{1i}. The wave height process $A_{1i}(t)$ is assumed to be a stationary Gaussian radom process with zero mean. A schematic representation of Eq. 2 is displayed in Fig. 1.

The intensity of the ith storm (wave height), $A_{1i}(t)$, is specified by its power spectral density that is a function of the storm wind velocity. Since $X_1(t)$ is a Poisson process, $A_{1i}(t)$ $(i=1,2,...)$ is statistically independent of $A_{1j}(t)$ for $i \neq j$. The duration of each storm, $T_{1i}(i=1,2,...)$, is a statistically independent and identically distributed random variable with the same average duration $\overline{T}_1$.

In Eq. 2, N_1 is the number of storms that occurr in the service time interval (0,t). It is a random variable with the Poisson distribution,

$$P[N_1=k] = \frac{(\lambda_1 t)^k e^{-\lambda_1 t}}{k!} \qquad (3)$$

Let p_1 be the probability of failure of a tower under a single storm, and E_1 be the event that the structure will survive such a storm. Then, the structural reliability, $L_1(t)$, under the application of the storm waves, $X_1(t)$, in the service time interval (0,t) is

$$L_1(t) = \sum_{k=0}^{\infty} P[E_1|N_1=k]\ P[N_1=k] \qquad (4)$$

Assuming that the resisting strength of the structure does not change with time (i.e., neglecting the strength degradation due to fatigue crack propagation), one obtains

$$P[E_1|N_1=k] = (1-p_1)^k \tag{5}$$

Substituting Eq. 3 and 5 into Eq. 4 and carrying out the summation, one obtains

$$L_1(t) = \sum_{k=0}^{\infty} (1-P_1)^k \frac{(\lambda_1 t)^k e^{-\lambda_1 t}}{k!} = e^{-\lambda_1 p_1 t} \tag{6}$$

in which p_1 is the probability of failure under a single storm, and it will be estimated later.

The fact that the occurrence of the storm waves, $X_1(t)$, is assumed to be ahomogeneous Poisson process implies that the storm occurrence is a chance event. Hence the distribution function of the time intervals between successive storms in negative exponential. Available storm data [e.g., Ref. 3] indicates that the interarrival times between successive storms follow the negative exponential distribution reasonably well, thus justifying the assumption of the homogeneous Poisson process for $X_1(t)$.

(ii) Structural Reliability $L_2(t)$ Under Strong Earthquakes $X_2(t)$

The earthquake process $X_2(t)$ is again modeled as a homogeneous Poisson process with an average occurrence rate λ_2 per year (or return period $1/\lambda_2$ years),

$$X_2(t) = \sum_{i=1}^{N_2} A_{2i}(t)\left[H(t-t_{2i}) - H(t-t_{2i} - T_{2i})\right] \quad (7)$$

in which $A_{2i}(t)$ is the ground motion process of the ith earthquake occurring at t_{2i} with a finite duration T_{2i}. $A_{2i}(t)$ can represent the ground acceleration $\ddot{U}_g(t)$, or the velocity $\dot{U}_g(t)$, or the displacement $U_g(t)$, depending on the design critera. $A_{2i}(t)$ is assumed to be a stationary Gaussian random process with zero mean, and hence it is specified by its power spectral density. A schematic figure for the ground acceleration is shown in Fig. 1. Since $X_2(t)$ is a Poisson process, the intensity of each earthquake is a statistically independent and identically distributed random variable. Furthermore, the duration of each earthquake, $T_{2i}(i=1,2,...)$, is also a statistically independent and identically distributed random variable having the same average duration $\bar{T}_2$.

Let p_2 be the probability of failure of the structure under a single earthquake. Then, in a similar fashion as for the case of storm waves, one obtains $L_2(t)$ as follows;

$$L_2(t) = e^{-\lambda_2 p_2 t} \quad (8)$$

(iii) Structural Reliability, $L_3(t)$, Under Simultaneous Occurrence of Earthquake and Storm, $X_3(t)$.

Since $X_1(t)$ and $X_2(t)$ are homogeneous Poisson process, it can be shown that the simultaneous occurrence of both processes, $X_1(t)$ and $X_2(t)$, denoted by $X_3(t)$,

is again a homogeneous Poisson process with an average occurence rate λ_3 per year (or return period $1/\lambda_3$ years).

The average occurrence rate λ_3 can be obtained from the average occurrence rates λ_1 and λ_2 as well as the average durations $\bar{T}_1$ and $\bar{T}_2$ of both $X_1(t)$ and $X_2(t)$ as follows [see derivations in Appendix I]

$$\lambda_3 = \lambda_1\lambda_2\left(\bar{T}_1 + \bar{T}_2\right) \tag{9}$$

Let p_3 be the probability of structural failure under a single occurrence of $X_3(t)$ (see Fig. 1). Then, in a similar manner, one obtains the probability of surviving $X_3(t)$ in the service time interval (0,t) as follows;

$$L_3(t) = e^{-\lambda_3 p_3 t} = e^{-\lambda_1\lambda_2\left(\bar{T}_1 + \bar{T}_2\right)p_3 t} \tag{10}$$

Substituting Eqs. 6, 8 and 10 into Eq. 1, one obtains the reliability, L(t), and the probability of failure, P(t), of the offshore towers in the service time interval (0,t) as,

$$\begin{aligned} L(t) &= \exp\left(-\lambda_1 p_1 t - \lambda_2 p_2 t - \lambda_3 p_3 t\right) \\ P(t) &= 1 - L(t) = 1 - \exp\left(-\lambda_1 p_1 t - \lambda_2 p_2 t - \lambda_3 p_3 t\right) \end{aligned} \tag{11}$$

It is observed from Eq. 11 that the reliability, $L(t)$, of the structure in $(0,t)$ depends on the probabilities of failure p_1, p_2 and p_3 under the single occurrence of storm waves $X_1(t)$, earthquakes $X_2(t)$, and both $X_3(t)$, respectively. These quantities will be estimated in the next section.

III. First Passage Failure Analysis

Since the applied loads to the structures resulting from a single occurrence of storm, $A_{1i}(t)$, earthquake , $A_{2i}(t)$, and both, $A_{3i}(t)$, are random processes, the dynamic structural responses, such as shear forces and bending moments, are also random processes. The estimation of the failure probability of the structure is within the scope of the first passage (or first excursion) analysis in random vibration [e.g., Refs. 44, 46-48].

Since $A_{1i}(t)$, $A_{2i}(t)$ and $A_{3i}(t)$ are assumed to be stationary Gaussian random processes, the structural responses are approximated by the stationary Gaussian random processes. Let $Z_1(t)$ be the response (either the shear force or the bending moment) at the critical location of the structure due to the storm waves $A_{1i}(t)$. Then, the response $Z_1(t)$ is completely specified by its power spectral density, denoted by $S_{Z_1Z_1}(\omega;W)$, where W is the average storm wind velocity appearing in the expression of the wave height spectrum as will be discussed later.

The average number of upcrossings per unit time, denoted by ν_1, for the response process $Z_1(t)$ over a strength level R is [e.g.,Ref. 44],

$$\nu_1 = \frac{\omega_1}{2\pi} e^{-R^2/2\sigma_1^2(W)} \tag{12}$$

in which $\sigma_1^2(W)$ is the variance of the response process $Z_1(t)$,

$$\sigma_1^2(W) = \int_{-\infty}^{\infty} S_{Z_1Z_1}(\omega;W)\, d\omega \tag{13}$$

and ω_1 is the apparent frequency of $Z_1(t)$,

$$\omega_1^2 = \int_{-\infty}^{\infty} \omega^2 S_{Z_1 Z_1}(\omega;W)\,d\omega \Big/ \int_{-\infty}^{\infty} S_{Z_1 Z_1}(\omega;W)\,d\omega \qquad (14)$$

Previous and current studies [Refs. 36-40] indicate that the apparent frequency of the response of the deep offshore towers can be approximated by the fundamental frequency ω_a of the tower, since the response spectrum $S_{Z_1 Z_1}(\omega;W)$ is narrow-banded.

Since the strength of the structure R is designed to be much larger than $\sigma_1(W)$, the failure rate h_1 (or risk function) per unit time can be approximated by $2\nu_1$

$$h_1 \simeq 2\nu_1 = \frac{\omega_a}{\pi}\, e^{-R^2/2\sigma_1^2(W)} \qquad (15)$$

in which ω_a is the fundamental natural frequency of the tower. Eq. 15 indicates that failure occurs when $Z_1(t)$ exceeds $|R|$ (two-sided thresholds). The approximation given in Eq. 15 is referred to as the Poisson approximation in random vibration [e.g., Refs. 44, 46-48], implying that the crossings (or excursions) over the strength $|R|$ are statistically independent. This type of approximation is consistent with the Poisson models assumed for the storm waves $X_1(t)$ and the earthquakes $X_2(t)$.

The total conditional failure rate during the ith storm (given the storm duration $T_{1i}=t_1$) is $h_1 t_1$. Since $T_{1i}(i=1,2,\ldots)$ is a statistically independent and identically distributed random variable with a probability density function $f_{T_1}(t)$,

the total failure rate, denoted by H_1, is

$$H_1 = \int_0^\infty h_1 t f_{T_1}(t)dt = h_1 \bar{T}_1 \qquad (16)$$

in which $\bar{T}_1$ is the average storm duration.

Thus, the probability of first passage failure under a single storm with the average storm wind velocity, W, and the structural strength, R, is

$$P_1^{**}(R,w) = 1 - e^{-H_1} = 1 - \exp\left\{-\frac{\omega_a \bar{T}_1}{\pi} e^{-R^2/2\sigma_1^2(w)}\right\} \qquad (17)$$

in which Eqs. 15 and 16 have been used. Eq. 17 is referred to as the exceedance probability per storm.

Since the resisting strength of the structure, R, is a random variable with a probability density function $f_R(x)$, the probability of first passage failure per storm, given an average storm wind velocity W=y, is

$$P_1^*(w=y) = \int_0^\infty f_R(x)\left\{1-\exp\left[-\frac{\omega_a \bar{T}_1}{\pi} e^{-x^2/2\sigma_1^2(W=y)}\right]\right\} dx \qquad (18)$$

Let $\sigma_2^2(S=z)$ be the variance of the structural response due to the earthquake ground motion, $A_{2i}(t)$, with an intensity S=z, and $\sigma_3^2(W=y, S=z)$ be the variance of the structural response due to the joint occurrence, $A_{3i}(t)$, of the storm (with an average storm wind velocity W=y) and the earthquake (with an intensity S=z). Then, in a similar fashion, the probabilities of first passage failure, $p_2^*(S=z)$ and $p_3^*(W=y, S=z)$, per earth-

quake (given S=z) and per joint occurrence of both (given W=y and S=z), respectively, can be shown as follows:

$$P_2^*(S=z) = \int_0^\infty f_R(x) \left\{ 1-\exp\left[-\frac{\omega_a \overline{T}_2}{\pi} e^{-x^2/2\sigma_2^2(S=z)} \right] \right\} dx$$

$$P_3^*(W=y, S=z) = \int_0^\infty f_R(x) \left\{ 1 - \exp\left[-\frac{\omega_a \overline{T}_3}{\pi} e^{-x^2/2\sigma_3^2(W=y, S=z)} \right] \right\} dx \qquad (19)$$

in which $\overline{T}_3$ is the average duration of the joint occurrence $A_{3i}(t)$, i.e., $\overline{T}_3 = \text{mini.}\ (\overline{T}_1, \overline{T}_2) = \overline{T}_2$.

The exceedance probability per earthquake, denoted by $P_2^{**}(R,S)$, follows from Eq. 17 as

$$P_2^{**}(R,S) = 1 - \exp\left\{ -\frac{\omega_a \overline{T}_2}{\pi} e^{-R^2/2\sigma_2^2(S)} \right\} \qquad (19\text{-a})$$

It should be mentioned that the probabilities of failure, $p_1^*(W=y)$, $p_2^*(S=z)$ and $p_3^*(W=y, S=z)$, per occurrence of storm, earthquake, and both, respectively, are conditional probabilities under the condition that the average storm wind velocity and the earthquake intensity are, respectively, W=y, S=z. The variances $\sigma_1^2(W=y)$, $\sigma_2^2(S=z)$ and $\sigma_3^2(W=y, S=z)$ of the Structural response appearing in Eqs. 18 and 19 will be obtained from the random vibration analysis of the offshore towers in the next section.

IV. Response Statistics to stochastic Storm Waves and Strong Earthquakes.

The equations of motion of an offshore tower considered as a lumped mass model is given by Eq. B-1 or B-4 of Appendix II. In Eq. B-4, $\{\dot{V}_0\}$ is the water particle velocity vector and $\{\ddot{U}_g\}$ is the ground acceleration vector [see Appendix II]. The statistical characterization of these excitations is discussed in the following:

(i) Spectra for Wave Height and Water Particle Velocity

The wind induced storm waves have been modeled as a stationary Gaussian random process with zero mean and finite duration, indicating that both the wave height and the water particle velocity are stationary Gaussian random processes. They are completely defined by their power spectral densities. In the present investigation, the Pierson-Moskowitz wave height spectrum [e.g., Ref. 14, 36-40] will be used

$$S_{hh}(\omega) = \frac{\alpha_1 g^2}{2|\omega|^5} \exp\left\{-\beta_1\left(\frac{g}{\omega W}\right)^4\right\} ; \quad -\infty<\omega<\infty \qquad (20)$$

in which α_1 and β_1 are nondimensional constants assumed to be 8.1×10^{-3} and 0.74, respectively; g is the acceleration of gravity; and W is the average storm wind velocity at a height of 64 ft above the sea surface.

The following cross-power spectral density of the water particle velocity vector $\left\{\dot{V}_0\right\}$ (Eq. B-4) is used [e.g.,Refs. 36-40];

$$S_{\dot{v}_j\dot{v}_k}(\omega) = \omega^2 S_{hh}(\omega) \frac{\cosh K(D-Y_j) \cosh K(D-Y_k)}{\sinh^2 KD} \quad (21)$$

in which D=depth fo water, ω=gKtanhKD, and Y_j=coordinate of jth lumped mass of the tower measured from the sea surface as shown in Fig. 2.

Eq. 20 indicates that the wave height spectrum depends on the average storm wind velocity W at 64' above the sea level. Since the wave height spectrum and hence the average storm wind velocity W vary from one storm to another in the design service life of the structure, W is a random variable. Since the storm waves $X_1(t)$ is a Poisson process, the average storm wind velocity W for each storm is a statistically independent and identically distributed random variable with a probability density function $f_W(x)$. This probability density function will be derived from available (measured) maximum wave height data in Seciton V.

(ii) Earthquake Ground Motion

A mentioned previously, the ground motion, $A_{2i}(t)$, such as the ground acceleration $\ddot{U}_g(t)$, velocity $\ddot{U}_g(t)$ and displacement $U_g(t)$, has been modeled as a stationary Gaussian random process with zero mean and finite duration.

The power spectral density of the horizontal ground acceleration $\ddot{U}_g(t)$ suggested in Ref. 30 and used in Refs. 36-40 will be employed herein.

$$S_{\ddot{u}_g\ddot{u}_g}(\omega) = \frac{1+4\zeta_g^2\left(\frac{\omega}{\omega_g}\right)^2}{\left[1-\left(\frac{\omega}{\omega_g}\right)^2\right]^2+4\zeta_g^2\left(\frac{\omega}{\omega_g}\right)^2} S^2 \qquad (22)$$

in which ω_g=characteristic ground frequency, ζ_g=characteristic ground damping ratio, and S^2=intensity of the power spectral density. For a firm soil condition, ω_g=15.6 rad/sec and ζ_g=0.6 was suggested in Ref. 30. Note that S^2 in Eq. 22 is equal to S_0 used in Ref. 36. It will be shown later that S is the intensity of the earthquake ground acceleration $\ddot{U}_g(t)$.

Since the earthquake intensity (or magnitude) varies from one earthquake to another in the design service life of the structure, S is a random variable. Since the earthquake process $X_2(t)$ is assumed to be a Poisson process, S for each earthquake is a statistically independent and identically distributed random variable with a probability density function $f_S(x)$. $f_S(x)$ will be derived from available (measured) earthquake records in Section V.

(iii) Response Variances $\sigma_1^2(W=y)$, $\sigma_2^2(S=z)$, and $\sigma_3^2(W=y, S=z)$

With the imput information given above, e.g., the earthquake ground acceleration spectrum (Eq. 22), the wave height spectrum (Eq. 20) and the cross-power spectral density of the water particle velocity (Eq. 21),

the system of equations of motion of the tower given by Eqs. B-13 and 14 is solved using the method of equivalent linearization technique discussed by Penzien et al [Refs. 36-40] in Appendix II. The variances of the shear force and the bending moment at each level of the lumped mass (see Fig. 2) are obtained in Eq. B-38 of the Appendix II. These response variances are associated with a particular average wind velocity, W=y, and a ground acceleration intensity, S=z. As a result, the response variances $\sigma_1^2(W=y)$, $\sigma_2^2(S=z)$, and $\sigma_3^2(W=y, S=z)$ required for the computation of the probabilities of failure given by Eqs. 18 and 19 are obtained from Eq. B-38 of the Appendix II.

It should be mentioned that the equations of motion of the offshore tower are nonlinear (Eq. B-1), which come from the effect of the drag force. It is time consumming to solve the nonlinear problem, since the iterative procedures should be used. Unfortunately, the effect of the drag force (or nonlinearity) is very important in the risk and reliability analysis of the offshore towers.

Under storm wave loading, the effect of drag force is negligible when the average storm wind velocity W is below 50 ft/sec.. The nonlinear effect increases as the average storm wind velocity W (or wave height) increases, and its effect is to increase the structural responses. The structural responses increases significantly at the high average storm wind velocity (or high wave height), by which the probability of failure of the structure is essentially contributed.

Under the earthquake loading, the nonlinear effect also increases as the intensity S of the ground acceleration increases. However, the nonlinear effect (drag force) under earthquake loading is to reduce (or retard) the structural response as will be shown later.

Although the response variance $\sigma_3^2(W=y, S=z)$ under the simultaneous occurrence of the storm and the earthquake has been obtained in the Appendix II, the numerical computations (including equivalent linearization, iteration and numerical integration) are quite time consumming. This comes from the fact that the peak frequencies of the ground acceleration spectrum and the water particle velocity spectrum usually lie on both sides of the fundamental frequency of the deep tower. Consequently, the response spectrum has to be computed at a large number of frequency points in the frequency domain in order to achieve a reasonable level of accuracy. Since the earthquakes are statistically independent of the storm waves, we have

$$\sigma_3^2(W=y, S=z) = \sigma_1^2(W=y) + \sigma_2^2(S=z) \tag{23}$$

provided that the equations of motion of the structure are linear. Eq. 23 is not valid when the equations of motion are nonlinear. However, our numerical results indicate that Eq. 23 can reasonably be used as an approximation. The maximum error associated with Eq. 23 is within 2% for large values of S and W. For small values of S and W, the error is within 0.5%. Hence, Eq. 23 will be used herein.

(iv) Unconditional Failure Probabilities.

It has been mentioned previously that the probabilities of first passage failure, $p_1^*(W=y)$, $p_2^*(S=z)$ and $p_3^*(W=y, S=z)$, are conditional, under the condition that the average storm wind velocity W is equal to y and the earthquake ground acceleration intensity S is equal to z, where both W and S are random variables. The unconditional probabilities of first passage failure (p_1, p_2 and p_3) due to a single occurrence of storm waves, earthquake, and both, respectively, can be obtained from the conditional probabilities [e.g., Refs. 7-9] as follows;

$$p_1 = \int_0^\infty p_1^*(W=y)\, f_W(y)\, dy$$

$$p_2 = \int_0^\infty p_2^*(S=z)\, f_S(z)\, dz$$

$$p_3 = \int_0^\infty \int_0^\infty p_3^*(W=y, S=z)\, f_W(y)\, f_S(z)\, dy\, dz \qquad (24)$$

in which $f_W(y)$ and $f_S(z)$ are the probability density functions of W and S, respectively, and $p_1^*(W=y)$, $p_2^*(S=z)$ and $p_3^*(W=y, S=z)$ are given by Eqs. 18 and 19.

Finally, the probability of failure or the reliability of the offshore tower in the service time interval (0,t) is obtained by substituting Eq. 24 into Eq. 11.

V. Statistical Distribution of Wave Height, Storm Wind Velocity, Ground Motion Intensity and Structural Strength

From Eqs.11 and 24, it is clear that in order to estimate the reliability of the offshore tower during its design service life, it is necessary to have the following information; (i) the average occurrence rates λ_1 and λ_2 and average durations, $\bar{T}_1$ and $\bar{T}_2$, of the storms and the earthquakes, respectively, and (ii) the probability density functions of the structural strength $f_R(x)$, the storm wind velocity $f_W(y)$, and the earthquake intensity $f_S(z)$. These information depend on the particular site of the structure (such as the North Sea, the Gulf of Alaska, the Gulf of Mexico, etc.) as well as the failure modes of the structure. They should be obtained or derived from available (measured) data as will be discussed in the following;

(i) Statistical Distribution of Structural Strength

An offshore platform can fail due to a variety of failure modes. Typical examples are deck leg failure, axial pile-soil failure including bearing failure or pull-out failure, lateral soil failure, pile bending failure, brace buckling, joint failure, pile-jacket connection failure, etc. A detailed discussion of various failure modes as well as the statistical distribution of the resisting strength associated with each failure mode has been presented for instance in Refs. 1-2. From the data presented in Ref. 1, the statistical dispersion (coefficient of variation) of the resisting

strength associated with various failure modes varies from about 5% for deck leg failure to about 20% for axial pile-soil failure. The statistical distribution of the resisting strength associated with each failure mode is assumed herein to be Weibull, i.e.,

$$f_R(x) = \frac{\alpha}{\beta}\left(\frac{x}{\beta}\right)^{\alpha-1} \exp\left(-\frac{x}{\beta}\right)^{\alpha} \qquad (25)$$

in which β is the characteristic strength (or scale parameter) and α is the shape parameter that is a measure of the coefficient of variation of the resisting strength. Hence, the probabilities of failure p_1, p_2 and p_3 appearing in Eq. 11 should be the summation of all the failure probabilities for all the failure modes in series [see Ref. 1].

(ii) Statistical Distribution of Expected Maximum Wave Height and Average Storm Wind Velocity

From the Pierson-Moskowitz wave height spectrum given by Eq. 20, the peak frequency, ω_p, occurs at

$$\omega_p = (4\beta_1/5)^{1/2}\,(g/W) \qquad (26)$$

indicating that the peak frequency depends on the average storm wind velocity W. It is noticed that the wave height spectrum is narrow-banded [see figures in Ref. 41].

The variance of the wave height, denoted by σ_h^2, is obtained by integrating the wave height spectrum to yield

$$\sigma_h^2 = \int_0^\infty S_{hh}(\omega)\,d\omega = \frac{1}{4}\frac{\alpha_1}{\beta_1}\frac{W^4}{g2} \tag{27}$$

From the extreme value theory, the statistical distribution of the maximum wave height can be approximated by the first asymptotic distribution of maximum value, with the expected maximum wave height, Y_{1m}, given by [e.g., Refs. 49-50, 31, 36].

$$Y_{1m} = K_1\,\sigma_h \tag{28}$$

$$K_1 = \left(2\ln\nu_w\overline{T}_1\right)^{1/2} + \left[0.5772\Big/\left(2\ln\nu_w\overline{T}_1\right)^{1/2}\right] \tag{29}$$

in which ν_w is the rate of upcrossings of zero mean (or the number of upcrossings over zero mean per unit time) given by

$$\nu_w = \frac{1}{2\pi}\left[\int_{-\infty}^{\infty}\omega^2 S_{hh}(\omega)\,d\omega\Big/\int_{-\infty}^{\infty}S_{hh}(\omega)\,d\omega\right]^{1/2} \simeq \frac{\omega_p}{2\pi} \tag{30}$$

Although ω_p and ν_w depend on W, K_1 given by Eq. 29 is not sensitive to the variation of W. Therefore, using W=100 ft/sec and $\overline{T}_1$=4 hours, we have $K_1 \simeq 3.85$. Furthermore, substitution of Eq. 27 into Eq. 28 yields

$$Y_{1m} \simeq C_1 W^2 \tag{31}$$

in which

$$C_1 = \frac{3.85}{2}\left(\frac{\alpha_1}{\beta_1}\right)^{1/2}\frac{1}{g} \tag{32}$$

Eq. 31 relates the expected maximum wave height, Y_{1m}, to the average (expected) storm wind velocity W at 64' above the sea surface. This relationship is plotted in Fig. 3.

Since both Y_{1m} and W vary from one storm to another, they are random variables. The distribution function of the expected maximum wave height Y_{1m}, denoted by $F_{Y_{1m}}(x)$, can be established from past records or hindcast, and is available,e.g.,in Refs. 1-3, 15-18. Therefore, the distribution function of W, denoted by $F_W(x)$, can be obtained from $F_{Y_{1m}}(x)$ through the transformation of Eq. 31 as follows;

$$F_W(x) = P\ [W \leq x] = P\left[\sqrt{Y_{1m}/C_1} \leq x\right] = F_{Y_{1m}}(C_1 x^2) \quad (33)$$

where C_1 is given by Eq. 32. The probability density function $f_W(x)$ can then be obtained from $F_W(x)$ by differentiation with respect to x.

It should be mentioned that in most of the literature, the significant wave height H_s is equal to $4\sigma_h$, i.e., $K_1=4.0$ in Eq. 29 [e.g., Refs. 18,19]. As a result, the average storm wind velocity W is related to the significant wave height through the relationship, $H_s=C_1^* W^2$ where $C_1^*=2(\alpha_1/\beta_1)^{1/2}/g$.

Some available distribution functions, $F_{Y_{1m}}(x)$, for the expected maximum wave height Y_{1m} in (i) the Gulf of Alaska, (ii) the North Sea, (iii) the Gulf of Mexico, and (iv) the Mustang Island, are given in Fig. 4 [from Refs. 2, 3, 11, 17, 18].

The distribution functions of the expected maximum wave height Y_{1m} in both the Gulf of Alaska and the North Sea have been characterized by the lognormal distribution in Refs. 2 and 11 (see Fig. 4). As a result, the distribution function of Y_{1m} can be written analytically as

$$F_{Y_{1m}}(x) = \Phi\left(\frac{\log x - \mu_w}{\sigma_w}\right) \tag{34}$$

in which $\Phi(\ )$ is the standardized normal distribution function. In Eq. 34, it is found that $\mu_w = 1.823$ and $\sigma_w = 0.095$ for the Gulf of Alaska, while $\mu_w = 1.867$ and $\sigma_w = 0.043$ for the North Sea (see Fig. 4) Curve (A), and $\mu_w = 1.762$ and $\sigma_w = 0.1$ for the North Sea Curve (B).

According to the transformation of Eq. 33, the probability density function of W can be shown as

$$f_W(y) = \frac{2\log e}{\sqrt{2\pi}\sigma_w y} \exp\left\{-\frac{1}{2}\left(\frac{\log c_1 y^2 - \mu_w}{\sigma_w}\right)^2\right\} \tag{35}$$

The corresponding probability density functions $f_W(y)$ given by Eq. 35 are presented in Figs. 5(a)-5(b).

On the other hand, however, the statistical distribution of the maximum wave height at some locations, e.g., the Mustang Island [Refs. 3, 18, 19] and the Gulf of Mexico Ref. 17] has been characterized by the first asymptotic distribution of maximum value,

$$F_{Y_{1m}}(y) = \exp\left\{-e^{-\frac{1}{\sigma^*}(y-\mu^*)}\right\} \tag{36}$$

in which it is found that $\mu^* = 25.944$ ft and $\sigma^* = 9.2$ ft for the Mustang Island, while $\mu^* = 41.53$ ft and $\sigma^* = 7.67$ ft for the Gulf of Mexico. In the case of Mustang Island, μ^* and σ^* are estimated from the probability plot displayed in Fig. 4(d). From the transformation of Eq. 33, the probability density function can be written as

$$f_W(y) = \frac{2C_1 y}{\sigma^*} \exp\left\{-\eta - e^{-\eta}\right\}$$

$$\eta = \frac{1}{\sigma^*}\left(C_1 y^2 - \mu^*\right) \tag{37}$$

The corresponding probability density functions, $f_W(y)$, are displayed in Figs. 5(c) and 5(d).

It is observed that from Figs. 4 and 5 that the storm wave is most severe in the Gulf of Alaska and least serious in the Mustang Island. The storm waves in the North Sea are also quite severe. Two different procedures have been used to estimate the frequency distribution of the maximum wave height in the North Sea thus resulting in two different distribution functions referred to as Curve (A) and Curve (B) [see Ref. 11], respectively. These two distributions will be used later to investigate their sensitivity with respect to the design of the offshore platforms.

(iii) Statistical Distribution of Expected Maximum Ground Acceleration and Earthquakes Intensity S.

The statistical distributions of the expected maximum ground acceleration, velocity and displacement are available

from past earthquake records in some areas [e.g.,Refs. 2, 24-30]. These distribution functions can be used to derive the probability density, $f_S(x)$, of the intensity S of the ground acceleration as follows;

The variance of the ground acceleration $\ddot{U}_g$, denoted by $\sigma^2_{\ddot{U}_g}$, is obtained from the integration of the power spectral density given by Eq. 22

$$\sigma^2_{\ddot{U}_g} = \int_{-\infty}^{\infty} S_{\ddot{U}_g \ddot{U}_g}(\omega)\, d\omega = \frac{\pi(1+4\zeta_g^2)\omega_g}{2\zeta_g} S^2 \qquad (38)$$

in which the contour integration technique in the complex plane has been used.

From the extreme value theory, the statistical distribution of the maximum ground acceleration can reasonably be approximated by the first asymptotic distribution of the maximum value [e.g., Refs. 31-36]. Hence, the expected maximum ground acceleration, denoted by Y_{2m}, is

$$Y_{2m} = E\left[\underset{t}{\text{maxi}} \left| \ddot{U}_g \right|\right] = K_2\, \sigma_{\ddot{U}_g} \qquad (39)$$

$$K_2 = \left(2 \ln \nu_g \overline{T}_2\right)^{1/2} + \left[0.5772 \Big/ \left(2 \ln \nu_g \overline{T}_2\right)^{1/2}\right]$$

in which ν_g is the rate of zero crossings, including up and down crossings, and is approximated by

$$\nu_g \simeq \omega_g / \pi \qquad (40)$$

Substitution of Eq. 38 into Eq. 39 leads to the relationship between the earthquake intensity S and the expected maximum ground acceleration Y_{2m}.

$$S = Y_{2m}/C_2 \tag{41}$$

in which

$$C_2 = K_2\left[\frac{\pi(1+4\ \zeta_g^2)\omega_g}{2\zeta_g}\right]^{1/2} \quad (2.54x12) \tag{42}$$

where the factor 2.54x12 is used to convert Y_{2m} from cm/sec^2 to ft/sec^2.

Eq. 41 relates the expected maximum ground acceleration, Y_{2m}, to the earthquake intensity, S. This relationship is displayed in Fig. 6. Furthermore, available distribution function of the expected maximum ground acceleration and velocity in the Gulf of Alaska are given in Fig. 7(a) and 7(b) [from Ref. 2], respectively.

When the distribution function, $F_{Y_{2m}}(x)$, of the expected maximum ground acceleration is available (see Fig. 7), the distribution function, $F_S(x)$, of the earthquake intensity S can be obtained from $F_{Y_{2m}}(x)$ through the transformation of Eq. 41 as follows;

$$F_S(z) = P\left[S \le z\right] = P\left[Y_{2m} \le C_2 z\right] = F_{Y_{2m}}(C_2 z) \tag{43}$$

The probability density, $f_S(z)$, of S can then be obtained from the distribution function, $F_S(z)$, by differentiation with respect to z.

Frequently, the records of the expected maximum ground motion may not be available, but the records of the earthquake magnitude in Richter scale are available. Under this circumstance, it is possible to derive the distribution function $F_{Y_{2m}}(x)$ from the statistical distribution of the earthquake magnitude in Richter scale [see, e.g., Ref. 31], and then $F_S(x)$ can be derived using Eq. 43.

It can be observed from Figs. 7(a) and 7(b) that the statistical distribution of the expected maximum ground acceleration is characterized by the lognormal distribution [Ref. 2],

$$F_{Y_{2m}}(x) = \Phi\left(\frac{\log x - \mu_s}{\sigma_s}\right) \tag{44}$$

in which x is in cm/sec^2, and $\mu_s = 1.758$, $\sigma_s = 0.297$.

Since the relationship between S and Y_{2m} is linear (Eq. 41), the probability density function of S, denoted by $f_S(z)$, is again lognormal.

$$f_S(z) = \frac{\log e}{\sqrt{2\pi}\sigma_s z} \exp\left\{-\frac{1}{2}\left(\frac{\log C_2 z - \mu_s}{\sigma_s}\right)^2\right\} \tag{45}$$

The probability density function of the earthquake intensity S in the Gulf of Alaska given by Eq. 45 is displayed in Fig. 8.

It should be mentioned that there are uncertainties involved in predicting the frequency distributions of both the expected maximum wave height and the expected maximum ground acceleration. These uncertainties should be accounted for if possible [e.g., Ref. 1], although the problem is not treated herein.

VI. Numerical Examples and Case Studies

Three deep offshore towers with the height of 1075 ft, 675 ft, and 475 ft, respectively, have been considered. These structures are modeled as lumped mass systems with 7 masses [Refs. 36-41]. A typical model is shown in Fig. 2.

The properties of each tower including (i) the mass [M], the volume [V], the area [A], and the depth Y associated with each node, (ii) the flexibility matrix $[K]^{-1}$, (iii) the total weight G, and (iv) the first three natural frequencies, are given in Tables 1-3. The damping matrix is chosen in such a way that the damping coefficient associated with each vibrational mode is 5%. The inertia coefficient K_M and the drag coefficient K_D are assumed to be 2.0 and 0.7 , respectively [Ref. 36].

With the input loading information of the wave height spectrum $S_{hh}(\omega)$(Eq. 20), the cross-power spectral density of the water particle velocity $S_{\dot{V}_j \dot{V}_k}(\omega)$(Eq. 21), and the power spectral density of the ground acceleration $S_{\ddot{U}_g \ddot{U}_g}(\omega)$(Eq. 22), the standard deviations of both the shear force and the bending moment at each mass level have been computed using the solution given by Eq. B-38 of the Appendix II. Only the standard deviations of the shear force and the bending moment at the base are presented herein. These quantities are displayed in Figs. 9 and 10, respectively, associated with different values of the average storm wind velocity W and the earthquake intensity S. The results neglecting the nonlinear

drag force (called linear solution) are also given for the purpose of comparison. It is observed that under earthquakes the effect of the nonlinear drag force is to reduce (retard) the structural response, and that the effect increases as the earthquake intensity or the depth of the tower increases. Furthermore, under storm waves the nonlinear drag force significantly increases the structural response at high storm wind velocity (large wave height).

From the available literature [e.g., Refs. 2,4], it appears that the base shear is an acceptable characterization of the gross effect on the structures, and it will be used herein. As mentioned previously, various failure modes should be considered in the reliability analysis. This, however, would involve the detail design of the towers as well as the load transfer mechanisms to each joint and detail. Therefore, it is assumed expediently that the base shear is a prime design quantity and other failure modes are designed accordingly.

The resisting strength, R, to the base shear is expressed in terms of the total weight (force), G, of the entire platform structure. The average duration $\bar{T}_1$ per storm is assumed to be 4 hours and the average duration $\bar{T}_2$ per earthquake is assumed to be 30 seconds for illustrative purposes.

The probabilities of failure, $p_1^{**}(R,W)$ (Eq. 17), per storm for specific values of the resisting strength, R, and specific values of the average storm wind velocity, W, are plotted in Figs. 11(a) and 11(b) for 1075' and 475' towers, respectively. The probabilities of failure, $p_2^{**}(R,S)$ [Eq. 19(a)], per earthquake associated with specific values of the resisting strength, R, and specific values of the earthquake intensity, S, are

plotted in Figs. 12(a) and 12(b). The curves shown in Figs. 11 and 12 are referred to as the exceedance curves. For instance, if the average storm wind velocity W is 120 ft/sec., (i.e., equivalent to 90' expected maximum wave height, see Fig. 3 and Eq. 31), and if the base shear resisting strength is 0.3G, the probability of failure per storm given by Fig. 11(a) is 0.2%. Note that the exceedance curves, Eqs. 17 and 19(a), are extremely easy to compute and they do provide a lot of information for the analysis and design purpose. Such information is very important in designing the aeronautical engineering structures.

The resisting strength R to the base shear is a random variable and is assumed to follow the Weibull distribution given by Eq. 25. The strength data associated with various failure modes given in Ref. 1 vary from about 5% for deck leg failure to about 20% for axial pile-soil failure. For illustrative purposes, the coefficient of variation of the resisting strength R to the base shear is assumed to be 10%, indicating that the shape parameter α is approximately 12 (see Eq. 25). The design characteristic strength β (or scale parameter), that is a central measure of the distribution depends on a particular design.

The probabilities of failure per storm, $p^*(W=y)$ given by Eq. 18, for different values of average storm wind velocities W and different design characteristic strength β (in terms of G) are plotted in Fig. 13. The probabilites of failure per earthquake, $p_2^*(S=z)$ given by Eq. 19, for different values of earthquake intensities S and design characteristic strength

β are also displayed in Fig. 14. For instance, if the average storm wind velocity W is 120 ft/sec., (i.e., 90 feet expected maximum wave height), the probability of failure for a design characteristic strength β=0.3G is found from Fig. 13a as 6.92%.

It has been shown previously that if the resisting strength is deterministic and is equal to 0.3G, the probability of failure under the same storm is 0.2%. The probability of failure increases to 6.92% when the statistical distribution of the resisting strength is accounted for (with 10% dispersion).

The probabilities of failure per storm p_1, per earthquake p_2, and per joint occurrence of both p_3(see Eq. 24) depend on the frequency distributions of both the earthquake intensity $f_S(z)$ (or the expected maximum ground acceleration) and the average storm wind velocity $f_W(y)$ (or the expected maximum wave height). These frequency distributions depend entirely on the geological location of the platform site, for instance, the Gulf of Alaska, the North Sea, the Gulf of Mexico, etc.

Using the probability density functions $f_W(y)$ and $f_S(z)$ obtained in Figs. 5 and 8 in the Gulf of Alaska, along with $p_1^*(W=y)$ and $p_2^*(S=z)$ presented in Figs 13 and 14, one obtains from Eq. 24 the probabilities of failure under one occurence of (i) storm p_1, (ii) earthquake p_2, and (iii) both storm and earthquake p_3. The results are displayed in Fig. 15.

In the Gulf of Alaska, that is a severe earthquake prone area, it is observed that the probability of failure due to a storm is several orders of magnitude larger than that due to an earthquake for three towers. This observation indicates that for the deep water platforms (e.g., above 300 ft. platform),

the earthquake loading is not important as compared to the storm waves and hence design for the storm wave will be sufficient for the earthquake loading. However, as the depth of the water decreases the storm wave spectrum that depends on the depth of the water will decrease and the importance of the earthquake loading will increase. Although we do not have enough structural data on short towers, it is expected that the earthquake loading may be as important as the storm waves when the water depth is less than 100 ft. The methodology of the analysis presented herein, however, can be applied to short towers as well.

It should be noticed that although the earthquake intensity S and the average storm wind velocity W, which appear in the earthquake ground acceleration spectrum $S_{\ddot{U}_g\ddot{U}_j}(\omega)$ and the wave height spectrum $S_{hh}(\omega)$, are used in the computation, they are related to the expected maximum ground acceleration and the expected maximum wave height through Eqs. 31 and 41, respectively (see also Figs. 3 and 6).

Another interesting observation is that although the joint occurrence of both the earthquake and the storm results in a larger structural response, i.e., $\sigma^2(W=y, S=z) \tilde{=} \sigma^2(W=y)+\sigma^2(S=z)$, the probability of failure due to the joint occurrence, p_3, is smaller than that due to the storm waves p_1. The reason is that the average duration $\bar{T}_3$ of the joint occurrence is $\bar{T}_3=\text{mini.}(\bar{T}_1,\bar{T}_2) = \bar{T}_2 = 30$ sec., while the average duration of the storm $\bar{T}_1$ is 4 hours. The significant difference in the loading duration is the only reason why p_3 may be smaller than p_1.

On the other hand, however, p_3 is always greater than p_2

because of equal average duration. It should be noticed that when the storm waves and the earthquake occur simultaneously, the structure continues to vibrate even after the earthquake stops. However, the probability of failure after the earthquake stops, has been accounted for in the Poisson process $X_1(t)$ of the storm wave already.

Consequently, it follows that p_3 is always greater than p_2, but p_3 may or may not be greater than p_1 depending on the relative magnitude of p_1 and p_2. As observed previously, if p_2 is several orders of magnitude smaller than p_1 then p_3 may be smaller than p_1 otherwise p_3 may be greater than p_1. As will be observed later that even if p_3 is greater than p_1 and p_2, it may not be important in the design, because its occurrence rate $\lambda_3$is at least three orders of magnitude smaller than the occurrence rates λ_1 and λ_2.

Furthermore, the probabilities of failure per storm p_1 vs. the design strength β in G (or design load) at various geological locations, i.e., the Gulf of Alaska, the Gulf of Mexico, the North Sea, and the Mustang Island, are presented in Fig. 16.

Having computed p_1, p_2 and p_3, we are now in the position to compute the probability of failure of the offshore platforms as a function of service time (0,t) using Eq. 11. For the Gulf of Alaska, the North Sea, and the Gulf of Mexico, the probability density functions $f_W(y)$ and $f_S(z)$ are the annual density functions, and hence $\lambda_1=\lambda_2=1$. For the Mustang Island, the occurrence rate of the storm λ_2 is 0.22[Ref. 3].

For the Gulf of Alaska, the probabilities of failure for the design strength β=0.4G are plotted in Fig. 17. The solid curves, designated by "wave", indicate the probability of failure due to the storm waves $X_1(t)$ alone, and the ordinate is given on the left hand side. The dashed curves, designated by "earthquake" and "joint", represent the probabilities of failure due to earthquakes $X_2(t)$, and the joint occurence $X_3(t)$, respectively. The ordinate of these two dashed curves are shown on the right hand side. Furthermore, the probability of failure for the design strength β=0.5G due to the storm waves $X_1(t)$ alone is also plotted as solid curve in Fig. 17 with the ordinate on the left hand side. It is observed that the probabilities of failure due to the earthquakes $X_2(t)$ and the joint occurrence $X_3(t)$ are several orders of magnitude smaller than that due to the storm wave $X_1(t)$, and hence they are negligible.

It is further noticed that although the probability of failure, p_3, due to a joint occurrence is one to two orders of magnitude greater than that due to an earthquake, p_2, the probability of failure in service due to the joint occurrence, $X_3(t)$, in the design service life is one order of magnitude smaller than that due to the earthquakes $X_2(t)$. This comes from the fact that the average occurrence rate λ_3 is much smaller than λ_2(see Eq. 9). It follows from Eq. 9 that if $\bar{T}_1$=4 hours, $\bar{T}_2$=30 sec., λ_1=1 and λ_2=1, then $\lambda_3=\lambda_1\lambda_2(\bar{T}_1+\bar{T}_2)\tilde{=}$ $4/365x24 = 0.457x10^{-3}$.

A conclusion can therefore be drawn from the present analysis that for the deep water offshore platforms, the design

for storm waves predominates, while the design for the earthquakes or the joint occurrences of both the earthquakes and storm waves is not important at all. For shallow water platforms (e.g., less than 100 ft.), the earthquake design may be of equal importance as the design for the storm waves in the severe earthquake areas. This will be investigated further. However, the joint occurrence of both the earthquakes and the storm waves is generally not important, because its occurrence rate λ_3 is about 3 orders of magnitude smaller than the occurrence rate λ_2 of the earthquakes. It may become important only if the earthquake design is important and at the same time the probability of failure of the offshore platform is specified to be very stringent, e.g., smaller than 1% in 20 years of design service life. Such a situation, however, is very unlikely. It is noticed that even in the severe earthquake zone of the Gulf of Alaska, the probability of failure due to the storm waves predominates for the deep water platforms (long period towers). Therefore, only the probabilities of failure due to the storm waves within 25 years of service life (t=25) vs. different design strength β are plotted in Fig. 18 for various geological locations.

It is observed from Fig. 18 that for a specified level of platform reliability in 25 years of service life, a higher design strength β (or design load) should be used in the Gulf of Alaska. For instance, if the platform reliability is specified to be 99% for the 1075' tower, the design characteristic strength β should be 0.467 G, 0.419 G, 0.392 G, 0.298 G and .22 G, respectively, for the Gulf of Alaska, the North

Sea (A), the North Sea (B), the Gulf of Mexico, and the Mustang Island. The results have been expected because of the relative severity of the frequency distribution function of the expected maximum wave height discussed previously and presented in Figs. 4 and 5.

Another observation from Fig. 18 is that for a specified level of reliability, the difference in the final design is rather small between two different frequency distributions of the expected maximum wave height at the North Sea, i.e., Curve A and Curve B. Both frequency distributions are estimated using two different procedures. Furthermore, the difference in the final design vanishes as the required level of reliability decreases. For instance, there is practically no difference in the design strength β (or load) if the specified reliability in 25 years of service life is smaller than 85% [see Fig. 18]. Even if the required level of reliability is high, such as 99 %, the difference in the design strength β (or load) is not substantial. As a result, it appears that the final design does not seem to be sensitive to the procedure for estimating the frequency distribution of the maximum wave height, if the probabilistic design procedure is employed. This conclusion may be of practical importance, since it has been of concern regarding the prediction procedures for the frequency distribution as well as the introduction of uncertainties (additional random variables) in the frequency distributions of the expected maximum wave height [Refs. 2, 11].

It has been observed from Figs. 11 to 18 that in order to maintain the same level of platform reliability, the design

strength β (or load), in terms of the total structural weight G, is much larger for the shallow towers than for the deep towers. For instance, if the platform reliability is specified to be 90% in the Gulf of Alaska, it follows from Fig. 18 that the design strength β is 0.375 G for the 1075' tower, while it is 0.7 G for the 475' tower.

Furthermore, the same situation holds not only for the storm wave loadings [see Figs. 11, 13, 15-18] but also for the earthquake loadings [see Figs. 12, 14-15]. For instance, the probability of failure per earthquake at an intensity of S= 0.234 ft/sec.^{2} rad$^{1/2}$ (that is equivalent to the El Central earthquake) is 0.56×10^{-3} for the 1075' tower at the design strength β=0.22G [see Fig. 14(a)]. To achieve the same level of failure probability for the 475' tower under the same earthquake, a design strength β should be 0.43 G [see Fig. 14 (b)].

Such a difference in design of the deep water platforms is of practical importance, and the reasons are explained in the following;

Under the wave loadings, the horizontal wave force is produced by the water particle velocity [see Eq. 11-1 of the Appendix II] which is specified by the cross-power spectral density $S_{\dot{v}_j \dot{v}_k}(\omega)$ (see Eq. 21). $S_{\dot{v}_j \dot{v}_k}(\omega)$ is the product of the wave height spectrum $S_{hh}(\omega)$ and an exponentially decay function of the distance from the sea surface for deep towers. An examination of the spectrum $S_{\dot{v}_j \dot{v}_k}(\omega)$ indicates that, for a given wave height spectrum $S_{hh}(\omega)$ (see Eq. 21), it is almost

the same at the sea surface for all deep towers. However, it decreases rapidly (exponentially) as the distance from the sea surface increases. Consequently, a large portion of the total horizontal wave forces is contributed by the water near the sea surface. This portion of the horizontal force does not differ much for deep towers of different height. Since the wave force decreases rapidly as the distance from the sea surface increases, the total horizontal wave force acting on the structure between 500' and 1000' from the sea surface is much smaller than that between 0' and 500' from the sea surface. This is the reason why the base shear of the tower does not increase proportionally with respect to its height and weight, and instead the shallow tower is subjected to large base shear force [see results presented in Fig. 9].

Under the earthquake loading, the excitation is applied to the base of the tower. The drag resistance (or retardation) of the water to the vibration of the tower depends on the velocity difference between the structure and the water particles. As a result, a deeper tower is subjected to a larger drag retardation than a shallow tower will experience, because of the depth of the water and the fundamental frequency of the tower [see Fig. 10].

The structural response of both the base shear and the bending moment under the storm waves and the earthquake loadings, respectively, have been presented in Figs. 9 and 10 in which both the linear solutions (neglecting the drag effect) and the nonlinear solutions (including the nonlinear drag effect) are displayed.

Fig. 10 clearly demonstrates that the 1075' tower experiences a substantial reduction in the base shear due to the beneficial drag retardation effect, while the 475' tower gains only a very small reduction in base shear from the drag effect. Furthermore, Fig. 9 indicates a tremendous increase in the structural response due to the nonlinear drag force under severe storm waves, e.g., $W \geq 100$ ft/sec. Unfortunately, the structural response in this region is extremely important in the reliability analysis as will be discussed later.

This appears to be the significant difference between the design of structures in water, such as the offshore platforms, and of structures on land, such as buildings. Under earthquake loadings, the buildings on land do not have the significant beneficial drag retardation effect (drag effect of air is negligible) and hence the response is reasonably linear. Consequently, the design in G loading (either design load or design strength) can be identical for both tall and short buildings. However, for the offshore platforms where the drag effect increases with respect to the height of the tower, a smaller design G loading can be used for the deeper tower and a larger design G loading should be used for the shallow tower in order to achieve the same level of reliability.

In the Gulf of Alaska it follows from Fig. 4(a) that the expected maximum wave height associated with a return period of 12.5 years is approximately 90 ft that is equivalent to the average storm wind velocity W=120 ft/sec [see Fig. 3]. Moreover, it follows from Fig. 7 that the expected maximum ground acceleration for a return period of 12.5 years is approximately 105 cm/sec^2 that corresponds to an earthquake intensity S=0.1031

$ft/sec^2 rad^{1/2}$ [see Fig. 6]. The standard deviations of the base shears under the storm waves W=120 ft/sec and the earthquake intensity S=0.1031 $ft/sec^2 rad^{1/2}$, respectively, are given in Table 4 for both nonlinear solutions and linear solutions (neglecting the drag force). These values are obtained from Figs. 9 and 10.

For the same return period, Table 4 clearly indicates that for the nonlinear solutions, the standard deviations of the base shear forces under sotrm waves are approximately 1.5 times that due to the earthquake. Hence, the design for storm waves predominates as discussed previously. However, if the nonlinear drag force is neglected (linear solutions) the standard deviations of the base shears under the earthquake is very close to those due to the storm waves (see Table 4). Consequently, the relative importance of the earthquake design increases drastically, although the design for the storm waves is still more important because of its long average duration $\overline{T}_2$. It is extremely important to notice from Table 4 that if the nonlinear drag force is neglected, the design is very unconservative and dangerous. As a result, it is concluded that the nonlinear drag force is extremely important in the design of deep offshore platforms.

VII. Conclusion and Discussion

A method of reliability assessment and design for the offshore platforms has been presented which combines the analyses of nonlinear random vibration and the first passage failure probability. The method presented herein is more rigorous than the conventional equivalent static or quasi static loading analyses.

In the present approach the storm waves and the earthquakes are modeled as homogeneous Poisson processes, while the joint occurrences of both the earthquakes and the storm waves is shown to be another homogeneous Poisson process with different occurrence rate. These three loading processes have been taken into account in the present analysis.

Historical data on the statistical distribution of the expected maximum wave height in the (i) Gulf of Alaska, (ii) Gulf of Mexico, (iii) North Sea, and (iv) Mustang Island, along with the earthquake data in the Gulf of Alaska have been employed to carry out the method of analysis presented herein. The probability of failure within any design service life has been obtained as a function of the designed load (or design strength) as well as many other variables, such as the statistical dispersion of the structural strength, the statistical distributions of the intensities and durations of both the storm waves and the earthquakes, etc.

For deep water offshore platforms (taller than 300 ft.), it is shown that the storm waves dominate the design criteria,

while the earthquake loading and the joint occurrence of both are not important. However, if the nonlinear drag force is neglected, the design becomes very unconservative and dangerous. It is, therefore, concluded that the nonlinear drag effect is extremely important in the design of deep offshore platforms and it must not be neglected.

The importance of the earthquake design relative to the wave design is expected to increase as the offshore tower becomes shorter. This is because the wave height spectrum will become less severe as the depth of the water decreases. The earthquake design may be as important as the wave design for the water depth less than 100 ft.

The joint occurrence of both the storm waves and the earthquakes is found to be unimportant in the design of deep offshore platforms. This is because the occurrence rate λ_3 is at least 3 orders of magnitude smaller than the occurrence rates λ_2 and λ_1 of the earthquakes and the storms, respectively. Although the joint occurrence produces a larger structural response, its duration is rather short (equal to the duration of the earthquake), and hence the failure probability per occurrence may be smaller than that due to the storm waves alone.

It has further been shown that unlike the structures on land, the design load (or design strength) in G loading (where G is the total weight of the structure) for the offshore

platforms should vary with respect to the depth of the tower in order to achieve the same level of reliability. For offshore platforms, the shorter tower should be designed at a much higher G loading than the taller tower. This situation is true whether the storm waves or the earthquakes dominate the design criteria.

The reason for such a difference come from the facts that (i) under the earthquake loading, the taller tower is subjected to a much larger nonlinear drag retardation in structural response from the water than the shorter tower, and (ii) under the wave loading, the wave forces acting on the structure diminish rapidly as the distance from the sea surface increases.

Two different procedures have been used in estimating the frequency distribution of the expected maximum wave height at the North Sea thus resulting in two different frequency distributions, referred to as Curve (A) and Curve (B) [see Figs. 4 and 5] (Ref. 11). However, it is found that the design based on two different frequency distribution is negligible if the reliability within 25 years of service life is specified to be smaller than 90%.

In the development of the present analysis, various assumptions and restrictions have been made which can be removed or relaxed in a more extensive subsequent study. Nevertheless, it is believed that the results presented herein are representative, and would not undergo major qualitative changes if these assumptions and restrictions are removed or relaxed, although quantitative changes would be expected as will be discussed in the following;

For simplicity of analysis, we consider only the firm soil foundation so that the interaction of the soil-pile-structure can be neglected. Such an interaction can be taken into account without any difficulty [e.g., Refs. 2, 4, 42, etc.]. However, the numerical computation for the random structural response will be much more involved, since the interaction is nonlinear.

The general effect of the soil-pile-structure interaction is to reduce the structural response under either the earthquakes or the storm waves or both. This is because the soil flexibility will absorb certain amount of energy of the applied loads thus alleviating the structural responses. Consequently, the numerical results presented in this report are conservative.

In the present analysis, the statistical distribution of the expected maximum ground acceleration of the earthquake records has been used [e.g., Ref. 2]. The information may not be available from the historical data which may contain only the statistical distribution of the earthquake magnitude in Richter scale [e.g., Refs. 24-33]. It has been mentioned previously, however, that the earthquake magnitude in Richter scale can be converted into the expected maximum ground motion [e.g., Ref. 31].

For a long period offshore platform, such as the deep water tower discussed herein, under earthquake excitations, it has been indicated in various papers [e.g., Refs. 2, 4, 25, etc.] that the structural responses computed based on the maximum ground velocity are more reasonable, and that the

structural responses computed based on the maximum ground acceleration input are too conservative. As a result, the numerical results presented herein are consistently conservative and it would be more reasonable to use the frequency distribution of the expected maximum ground velocity displayed in Fig. 7(b). For expediency, we employed an empirical ground acceleration spectrum, Eq. 22, that has been used by many researchers [e.g., Refs. 30-40]. Unfortunately, when the acceleration spectrum, Eq. 22, is converted into the velocity spectrum, the variance of the velocity does not converge [Ref. 31]. Hence, another empirical ground velocity spectrum should be used [e.g., Ref. 31] if the maximum ground velocity is to be used for the design purpose.

It is very important to emphasize, however, that even with the use of the ground acceleration spectrum along with the frequency distribution of the maximum ground acceleration [Fig. 7(a)] input for the earthquake excitations, which is too conservative, we have shown that the earthquake design is not important at all for the long period offshore platforms (i.e., deep towers) as compared to the wave design. This point is of significant importance.

The Pierson-Moskowitz wave height spectrum, Eq. 20, has been used in the random vibration analysis to obtain the structural responses. The wave height spectrum depends on the water depth, the fetch length, the storm duration, etc. The particular parameter values of α_1 and β_1 used in Eq. 20 are appropriate for deep water in the open sea. For shallow water with finite fetch length, the values of α_1 and β_1 should

be changed accordingly. Furthermore, the wave height spectrum becomes less severe as the water depth decreases.

It has been of concern that the sea wave spectrum may not be continuous such as Eq. 20. It may contain discrete components in the frequency domain as observed from the measured data. The effect of discrete sea wave spectrum on the structural response will be discussed in the next report.

It has been discussed in the literature that there are uncertainties associated with the estimation of both the wave and the earthquake spectra. These uncertainties may be contributed by the incomplete histroical data, hindcast techniques, and others. They should be taken into account if possible [e.g., Ref. 1].

Under severe storm waves or strong earthquakes, some parts of the structure may yield. The effect of the inelastic behavior under severe environmental loads should be investigated. Furthermore, the resisting strength of the structure to the earthquake loading may be different from that of the structure to the storm waves. This problem should be investigated based on the detailed design of the towers.

The earthquake loading has been modeled as a stationary random process with a finite duration because of simplicity in analysis [e.g., Refs. 28-43]. It is well-known, however, that the earthquake ground motion is nonstationary. The nonstationary effect and the effect of yielding on the response of the offshore platforms has also been investigated [Ref. 51].

The Pierson-Moskowitz spectrum used in the analysis is

a fully developed sea spectrum. However, the storm waves are developed gradually in time. It has been noticed that when the wave trains hit a member that is at rest, a significant impact loading on the structure has been observed. Such an impact loading may be of practical importance in the design of platforms and it is a subject of our further study.

We have not investigated the wave loadings induced by earthquakes or tsunami. However, the effect of current on the structural response has been investigated recently [Ref. 52]. It is shown in Ref. 52 that the effect of current may not be important.

The most serious assumption of the present investigation in assessing the offshore platform reliability is that the fatigue failure mode has been neglected. Fatigue is an important problem and it has received considerable attention. Even under the moderate sea waves, the fatigue cracks at some joints may propagate thus resulting in local failure, if not catastrophic failure due to the redundancies of the structure. However, as local failure occurs due to fatigue, the residual strength of the entire structure decreases thus increasing the failure rate (risk function) and the probability of catastrophic failure [e.g., Refs. 53-54]. This is a subject of our further investigation.

As the fatigue damage accumulation increases and the local joints damaged, the repair procedure has to be developed in order to maintain the prescribed level of structural reliability and integrity. The inspection and repair maintenance procedures may be expensive. This is a subject

of further investigation with respect to the cost optimization [e.g., Refs. 55-56].

In the present investigation, the total weight G and the stiffness matrix of the structure are considered to be constant, independent of the design strength β (or design load). This is only an approximation, since the total structural weight and stiffness will increase slightly as the design strength (or load) increases. It is a classical iterative process. However, the investigation of such an iterative procedure can only be made for a particular structure in the stage of the detail design, which is not the purpose of the present paper.

Page 49 intentionally blank

References

1. Stahl, B., "Probabilistic Methods For Offshore Platforms," presented at the 1975 Annual Meeting, Division of Production, American Petroleum Institute, Texas, April 1975, API paper No. 364-J.

2. Bea, R.G., "Earthquake Criteria for Platforms in the Gulf of Alaska," Offshore Technology Conference, Dallas, Texas, Paper Number OTC 2675, 1976.

3. Schueller, G.I., "On the Risk Assessment of Offshore Structures," Offshore Technology Conference, Dallas, Texas, Paper Number OTC 2334, 1975.

4. Marshall, P.W., "Risk Evaluations for Offshore Structures," Journal of the Structural Division, ASCE, Vol. 95, No. ST12, Dec. 1969.

5. Freudenthal, A.M., "Safety and the Probability of Structural Failure," Transactions ASCE, 1956.

6. Freudenthal, A.M., "Safety, Reliability, and Structural Design," Journal of the Structural Division, ASCE, March 1961.

7. Freudenthal, A.M., Gaüelt, J.M., and Shinoznke, M., "The Analysis of Structural Safety," Journal of Structural Division, ASCE, Vol. 92, No. ST1, 1966, pp. 267-325.

8. Benjamin, J.R., and Cornell, C.A., Probability, Statistics and Decision For Civil Engineers, McGraw-Hill, 1970, New York.

9. Ang, A.H.S., and Tang, W.H., Probability Concept in Engineering Planning and Design, John Wiley and Son, New York, 1975.

10. Freudenthal, A.M., and Gaither, M.S.; "Design Criteria for Fixed Offshore Structures," Preprints, Offshore Technology Conference Paper No. 1058, 1969.

11. Bea, R.G., "Selection of Environmental Criteria for Offshore Platform Design," Paper OTC 1839, Offshore Technology Conference, Houston, Texas, 1973; also, Journal of Petroleum Technology, Vol. XXVI, 1974.

12. Bea, R.G., "Development of Safe Environmental Criteria for Offshore Structures," presented at the 1975 Oceanology International Exhibition, Brighton, England, March 1975.

13. Marshall, P.W., and Bea, R.G., "Failure Modes of Offshore Platforms," presented at the ASCE-EMD Speciality Conference on Probabilistic Methods in Engineering, Stanford University, June 1974.

14. Pierson, W.J. Jr., and Moskowitz, L.A., "A Proposed Spectral Form For Fully Developed Wind Seas Based on Similarity Theory of

15. Hsu, F.H., "Hindcast Storm Waves for Compilation of Wave Statistics," Paper SPE 4324, Second Annual European Meeting of the Society of Petroleum Engineers of AIME, London, England, 1973.

16. Nolte, K.G., "Statistical Methods for Determining Extreme Sea States", Second International Conference on Port and Ocean Engineering Under Artic Conditions, University of Iceland, August 1973.

17. Bea, R.G., "Gulf of Mexico Hurricane Wave Heights," Paper OTC 2110, Offshore Technology Conference, Houston, Texas, 1974.

18. Russell, L.R., and Schuëller, G.I., "Probabilistic Models for Texas Gulf Coast Hurricane Occurrences," J. Petroleum Techn., March 1974.

19. Ourning, P.J., "Prediction of Maximum Wave Height from Historical Data," Preprints, Offshore Technology Conference Paper No. 1343, April, 1971.

20. Jahns, H.O., and Wheeler, J.D., "Long Term Wave Probabilities Based on Hindcasting of Severe Storms," Preprints, Offshore Technology Conference, Paper No. 1590, May 1972.

21. Quayle, R.G. and Fulbright, D.C., "Extreme Wind and Wave Return Periods for the U.S. Coast," Mariners Weather Log, Nat. Oceanic and Atmos. Admin., March, 1975.

22. Thom, H.C.S., "Extreme Wave Height Distributions Over Oceans," J. of Waterways, Harbors and Coastal Eng. Div., ASCE, 1973.

23. Cardone, V.J., Pierson, W.J., and Ward, E.G., "Hindcasting the Directional Spectra of Hurricane Generated Waves," Offshore Technology Conference, Paper No. OTC 2332, 1975.

24. Wiggins, H.H., Hasselman, T.K., and Chrostowski, H.D., "Seismic Risk Analysis for Offshore Platforms in the Gulf of Alaska," Offshore Technology Conference, Dallas, Texas, Paper Number OTC 2669, 1976.

25. Cornell, C.A. and Vanmaroke, E.H., "Seismic Risk Analysis for Offshore Structures," Offshore Technology Conference, Dallas, Texas, Paper Number OTC 2350, 1975.

26. Page, R.A., "Evaluation of Seismicity and Earthquake Shaking at Offshore Sites," Offshore Technology Conference, Paper No. OTC 2354, 1975.

27. Idriss, I.M., Dobry, R., and Power, M.S., "Soil Response Considerations in Seismic Design of Offshore Platforms," Offshore Technology Conference, Paper No. OTC 2355, 1975.

28. Hassekman, T.K., Bronowicke, A., and Chrostowski, J. "Probabilistic Response of Offshore Platforms to Seismic Excitation," Offshore Technology Conference, Paper No. OTC 2353, 1975.

29. Kirkley, C.M. and Murtha, J.P. "Earthquake Response Spectra for Offshore Structures," Offshore Technology Conference, Paper No. OTC 2356, 1975.

30. Kanai, K., "Semi-Empirical Formula For the Seismic Characteristics of the Ground," Bull Earthquake Research Institute, Tokyo, Japan, Vol. 35, June 1967, pp. 308-325.

31. Shinozuke, M., "Method of Safety and Reliability Analysis," International Conference on Structural Safety and Reliability, Edited by A.M. Freudenthal, Pergamon Press, 1969.

32. Tajimi, H. "A Structural Method of Determining the Maximum Response of a Building Structure During an Earthquake," Pro., Second World Conf. Earthquake Engineering, Tokyo and Kyoto, Japan, July, 1960.

33. Housner, G.W., "Strong Ground Motion," Earthquake Engineering (Edited by R.L. Wiegel), Prentice Hall (1970).

34. Clough, R.W., "Earthquake Response of Structures," Chapt. 4, pp. 75-91. Earthquake Engineering, Edited by R.L. Wiegel, Chapt. 12, pp. 307-334, Prentice Hall 1970.

35. Page, R.A., Boore, B.M., Joyner, W.B., and Coulter, J.W., "Ground Motion Values for Use in the Seismic Design of the Trans-Alaska Pipeline System," Geological Survey Circular 672, 1972.

36. Penzien, J., Kaul, M.K., and Borge, B., "Stochastic Response of Offshore Towers To Random Sea Waves and Strong Motion Earthquakes," Journal of Computer and Structures, Vol. 2, 1972, pp. 733-756.

37. Malhotra, A.K., and Penzien, J., "Nondeterministic Analysis of Offshore Structures," Journal of Engn. Mech. Div., ASCE, Dec. 1970, pp. 985-1003.

38. Malhotra, A.K., and Penzien, J., "Response of Offshore Structures to Random Wave Forces," Journal of Structural Div., ASCE, Oct. 1970, pp. 2155-3273.

39. Malhotra, A.K., and Penzien, J., "Response of Offshore Towers To Earthquake Excitation," Proc. Civil Engineering in the Oceans II, ASCE, Dec. 1969, pp. 65-76.

40. Penzien, J., and Liu, S.C., "Nondeterministic Analysis of Nonlinear Structures Subjected To Earthquake Excitations," Proc. 4th World Conference on Earthquake Engineering, 1969.

41. Shinozuka, M., Yun, C., and Vaicaitis, R. "Dynamic Analysis of Fixed Offshore Structures Subjected To Wind Generated Waves," Technical Report No. 7, Columbia University, prepared for NSF Under Grant No. NSF GK 37271X, March 1976.

42. Penzien, J. (1970), "Soil-Pile Foundation Interaction," Earthquake Engineering, R.L. Wiegel Editor, Prentice-Hall.

43. Penzien, J., "Seismic Analysis of Platform Structure-Foundation Systems," Offshore Technology Conference, Paper No. OTC 2352, 1975.

44. Lin, Y.K., "Probabilistic Method in Structural Dynamics," McGraw-Hill, 1967.

45. Kryloff, N., and Bogoliuboff, N., Introduction To Nonlinear Mechanics: "Approximate Asymoptotic Methods," Princeton University Press, 1947.

46. Lin, Y. K., "On the First Excursion Probability of Randomly Excited Structures: II," AIAA Journal, Vol. 8, No. 10, 1970, pp. 1888-1890.

47. Yang, J. N., and Shinozaka, M., "On the First Excursion Probability in Stationary Narrow-Band Random Vibration II," Journal of Applied Mechanics, ASME, Vol. 39, No. 3, 1972, pp. 733-738.

48. Yang, J. N., "Approximation To First Passage Probability," Journal of Engineering Mechanism Division, ASCE, Vol. 101, No. EM4, 1975, pp. 361-372.

49. Davenport, A. G., "Note on the Distribution of the Largest Value of a Random Function with Application to Gust Loading," Proc. of Inst. Civil Engineers, 1963.

50. Gumbel, E. J., Statistics of Extremes, Columbia University Press, New York, 1958.

51. Kaul, M. K., and Penzien, J.,"Stochastic Seismic Analysis of Yielding Offshore Towers," J. of Eng. Mech. Divi., ASCE. Vol. 100, No. EMS, 1974, pp. 1025-1037

52. Wu, S. C., "The Effect of Current on Dynamic Response of Offshore Platforms," Offshore Technology Conference, Dallas, Texas, Paper No. OTC 2540, 1976.

53. Yang, J. N., and Heer, E., "Reliability of Randomly Excited Structures," AIAA Journal, Vol. 9, No. 7, 1971, pp. 1262-1268.

54. Yang, J. N., and Trapp, W. J., "Reliability Analysis of Aircraft Structures Under Random Loading and Periodic Inspection," AIAA Journal, Vol.12, No. 12, 1974, pp. 1623-1630.

55. Yang, J. N., and Trapp, W. J., "Inspection Frequency Optimization for Aircraft Structures Based on Reliability Analysis," Journal of Aircraft, AIAA, Vol. 12, No. 5, 1975, pp. 494-496.

56. Yang, J. N., "Statistical Estimation of Service Cracks and Maintenance Cost for Aircraft Structures," Journal of Aircraft, AIAA, Vol. 13, No. 12, 1976, pp. 1041-1057.

57. Parzen, E., Stochastic Processes, Holden-Day, Inc., 1964.

58. Wen, Y. K., "Probability of Extreme Load Combination," Presented at the 4th International Conference on Structural Mechanics in Reactor Technology, San Francisco, August, 1977.

Appendix I: Derivation of Average Occurrence Rate λ_3 For Simultaneous Occurrence of Storm Waves and Earthquakes

For the sake of simplicity in derivation, we first consider the special case where the average duration of storm waves $\overline{T}_1$ is much greater than that of the earthquake $\overline{T}_2$, i.e., $\overline{T}_1 >> \overline{T}_2$. Such a restriction will then be removed later. The total duration in which $X_1(t)$ occurs in the service interval $(0,t)$, denoted by D_1, is

$$D_1 = \sum_{i=1}^{N_1} T_{1i} \qquad \text{(A-1)}$$

in which N_1 is a random variable denoting the total number of occurrences of storms in $(0,t)$, and T_{1i} is the duration of the ith storm. D_1 is recognized as a Compound Poisson process [e.g., Ref. 57]. The average value of D_1 is obtained from Eq. A-1 as

$$E[D_1] = \lambda_1 t \overline{T}_1 \qquad \text{(A-2)}$$

Let N_3 be the total number of occurrences of earthquakes $X_2(t)$ in the time interval D_1 (when the storm waves $X_2(t)$ occur). Then, N_3 is the total number of simultaneous occurrences of $X_3(t)$. The average number of N_3 can be obtained as follows

$$E[N_3] = E\{E[N_3|D_1]\} = E[\lambda_2 D_1] \qquad \text{(A-3)}$$

Substituting Eq. A-2 into Eq. A-3, one obtains

$$E[N_3] = \lambda_1 \lambda_2 t \, \bar{T}_1 \tag{A-4}$$

When the duration of the earthquakes $X_2(t)$ is not small compared to that of the storm waves $X_1(t)$, it can be shown by symmetry that

$$E[N_3] = \lambda_1 \lambda_2 t (\bar{T}_1 + \bar{T}_2) \tag{A-5}$$

As a result, the average occurrence rate λ_3 for the Poisson process $X_3(t)$ is

$$\lambda_3 = E[N_3]/t = \lambda_1 \lambda_2 (\bar{T}_1 + \bar{T}_2) \tag{A-6}$$

It is mentioned that in the design of nuclear reactor structures, the joint occurrence of several loads may occur and similar technique for the extreme load combination has also been investigated [e.g., Ref. 58].

Appendix II: Random Vibration of Offshore Platforms

The analysis techniques for random vibration of the offshore platforms used herein follow essentially the same approach presented by Penzien, et al, i.e., the method of equivalent linearization [Refs. 36-45]. However, some modifications have been made from the view point of frequency domain analysis, and the solution is expressed in terms of matrix operation for convenience in computer coding. It is mentioned that the numerical results obtained using the method of equivalent linearization have been shown recently to be reasonably accurate as compared to the results obtained by the method of Monte Carlo simulation [Ref. 41]. Furthermore, the excitation due to current has also been shown to be unimportant recently [Ref. 51]; hence it will be neglected in the present analysis.

(i) Equations of Motion and Linearization

For an offshore tower modeled as a lumped mass system with N degrees of freedom, the dynamic equations of motion can be written in the matrix form [Ref. 36-40]

$$[M]\{\ddot{U}_t\}+[C]\{\dot{U}\}+[K]\{U\} = \rho(K_M-1)[V]\{\ddot{V}_0-\ddot{U}_t\}+\rho[V]\{\ddot{V}_0\}$$

$$+\rho K_D[A]\{(\dot{V}_0-\dot{U}_t)|\dot{V}_0-\dot{U}_t|\} \qquad (B\text{-}1)$$

in which vectors $\{\dot{V}_0\}$ and $\{\ddot{V}_0\}$ represent water particle

velocities and accelerations, respectively; vectors $\{\dot{U}_t\}$ and $\{\ddot{U}_t\}$ represent the total structure velocities and accelerations, respectively, from a fixed reference; vectors $\{\dot{u}\}$ and $\{U\}$ represent the structure velocities and displacements, respectively, as measured relative to its moving base; diagonal matrices [M], [V], and [A] represent the structural lumped masses, volumes, and areas, respectively; matrices [C] and [K] represent structural damping and stiffness coefficients, respectively (foundation effects may be included); and ρ, K_M and K_D are scaler quantities representing the mass density of the water, the inertia coefficient, and the drag coefficient, respectively. While coefficients K_M and K_D are normally considered constants having values in the ranges $1.4 \leq K_M \leq 2.0$ and $0.5 \leq K_D \leq 0.7$, they may vary considerably for oscillating structures and may be frequency dependent [Ref. 46]. In this particular investigation K_M and K_D are assumed constant and equal to 2.0 and 0.7, respectively, as used in Ref. 46.

Let $\{U_g\}$ be a vector in which each component is the same time history of horizontal ground displacement. Then,

$$\{U_t\} = \{U\} + \{U_g\} \tag{B-2}$$

Introducing a relative displacement vector{r}

$$\{r\} = \{V_0\} - \{U_t\} \tag{B-3}$$

and substituting Eqs. B-2 and B-3 into Eq. B-1, one obtains

$$[m]\{\ddot{r}\}+[C]\{\dot{r}\}+[K]\{r\}+\rho K_D[A]\{\dot{r}|\dot{r}|\}$$
$$= [M-\rho V]\{\ddot{V}_0\}+[C]\{\dot{V}_0\}+[K]\{V_0\}-[C]\{\dot{V}_g\}-[K]\{V_g\} \quad \text{(B-4)}$$

in which

$$[m] = [M+\rho(K_M-1)V] \quad \text{(B-5)}$$

is the modified mass matrix of the tower in water.

If each component of the nonlinear vector $\{\dot{r}|\dot{r}|\}$ is linearized by the method of equivalent linearization [Refs. 36, 44-45] i.e., $\dot{r}_j|\dot{r}_j|$ is replaced by $a_j\dot{r}_j$, then the error e_j resulting from such an approximation is

$$e_j = \dot{r}_j|\dot{r}_j| - a_j\dot{r}_j \quad \text{(B-6)}$$

in which a_j will be determined such that the mean square error $E[e_j^2]$ is minimized.

Minimizing the mean square error, i.e., setting $E[\partial e_j^2/\partial a_j] = 0$ and solving for a_i, one obtains

$$a_j = E[\dot{r}_j^2|\dot{r}_j|]/E[\dot{r}_j^2] \quad \text{(B-7)}$$

Consequently, the vector $\{\dot{r}|\dot{r}|\}$ in Eq. B-4 can be replaced by $[a]\{\dot{r}\}$. This replacement results in an equivalent (optimal) damping matrix $[\hat{C}]$,

$$[\hat{C}] = [C] + \rho K_D [A][a] \tag{B-8}$$

Thus, one obtains the linearized equations of motion as follows;

$$[m]\{\ddot{r}\}+[\hat{C}]\{\dot{r}\}+[K]\{r\} = [M-\rho V]\{\ddot{V}_0\}+[C]\{\dot{V}_0\}+[K]\{V_0\}$$

$$-[C]\{\dot{U}_g\}-[K]\{U_g\} \tag{B-9}$$

Since both the ground motion and the water particle velocity are modeled as Gaussian random processes with zero mean, the response of the linearized equations of motion (Eq. B-9) is also a Gaussian process. Consequently, the probability density function of $\dot{r}_j$, denoted by $f_{\dot{r}_j}(x)$ is Gaussian with zero mean and standard deviation $\sigma_{\dot{r}_j\dot{r}_j}$ i.e., $f_{\dot{r}_j}(x) = \phi(x/\sigma_{\dot{r}_j\dot{r}_j})$ where $\phi()$ is the standardized Gaussian density function. With the aid of $f_{\dot{r}_j}(x)$, a_j appearing in Eq. B-7 can be evaluated as $\rho K_D A_i \sigma_{\dot{r}_j\dot{r}_j}\sqrt{8/\pi}$. As a result, Eq. B-8 becomes

$$[\hat{C}] = [C] + [\bar{C}] \tag{B-10}$$

in which

$$\bar{C}_{ij} = \begin{cases} 0 & ; \ i \neq j \\ \rho K_D A_j \sigma_{\dot{r}_j\dot{r}_j}\sqrt{8/\pi} & ; \ i=j \end{cases} \tag{B-11}$$

Substitution of Eq. B-2 into Eq. B-3 yields

$$\{r\} = \{V_0\} - \{U\} - \{U_g\} \tag{B-12}$$

We now substitute Eq. B-12 back into Eq. B-9 to obtain the linearized equations of motion in $\{U\}$

$$[m]\{\ddot{U}\}+[\hat{C}]\{\dot{U}\}+[K]\{U\} = \{F(t)\} \tag{B-13}$$

in which

$$\{F(t)\} = [\rho K_M V]\{\ddot{V}_0\}+ [\bar{C}]\{\dot{V}_0\}-[m]\{\ddot{U}_g\}-[\bar{C}]\{\dot{U}_g\} \tag{B-14}$$

Note that the components of $[\hat{C}]$ and $[\bar{C}]$ involve $\sigma_{\dot{r}_j\dot{r}_j}$ (j=1,2,...n) that is the solution of Eq. B-12 yet to be determined. Therefore, an iterative procedure should be employed starting with the linear solution $\sigma_{\dot{r}_j\dot{r}_j}=0$ (i.e., neglecting the effect of drag force). The convergence of such an iterative procedure appears to be very rapid.

(ii) Frequency Response Function

To calculate the response statistics, the normal mode superposition is used

$$\{U\} = [\phi]\{Y\} \tag{B-15}$$

in which $\{Y\}$ is the normal coordinate vector, and $[\phi]$ is the

modal matrix obtained from the undamped homogenous equations of Eq. B-13.

Premultiplying Eq. B-13 by $[\phi]^T$, and using Eq. B-15 and the orthogonality conditions, one obtains the equations of motion as follows;

$$[M^*]\{\ddot{Y}\}+[C_0]\{\dot{Y}\}+[K^*]\{Y\} = \{P\} \tag{B-16}$$

in which

$[M^*] = [\phi]^T[m][\phi]$ = generalized mass matrix

$[K^*] = [\phi]^T[K][\phi] = \omega^2[M^*]$ = generalized stiffness matrix

$[C_0] = [\phi]^T[\hat{C}][\phi]$ = coupled damping matrix

$\{P\} = [\phi]^T\{F(t)\}$ = generalized force vector

It follows from equation B-10 that $[C_0]$ is not diagonal, even though the original damping matrix [C] is chosen such that $[\phi]^T[C][\phi]$ is diagonal.

In order to uncouple Eq. B-16, another equivalent linearization technique is used. The term $[C_0]\{\dot{Y}\}$ is replaced by $[C^*]\{\dot{Y}\}$ where [C*] is diagonal and the element of [C*] is determined by minimizing the mean equare error vector $\hat{e}$

$$\{\hat{e}\} = [C_0]\{\dot{Y}\} - [C^*]\{\dot{Y}\} \tag{B-17}$$

It can be shown, after minimization, that

$$C_j^* = \sum_{k=1}^{N} \frac{C_{0jk}E[\dot{Y}_j\dot{Y}_k]}{E[\dot{Y}_j^2]} \tag{B-18}$$

Thus, Eq. B-16 is uncoupled and each equation can be written as

$$M_j^* \ddot{Y}_j + C_j^* \dot{Y}_j + K_j^* Y_j = \sum_{k=1}^{N} \phi_{jk}^T F_k(t) \qquad \text{(B-19)}$$

Note that C_j^* in Eq. B-19 involves $E[\dot{Y}_j Y_k]$ that is the solution of Eq. B-19 yet to be determined. Consequently, another iterative procedure should be used until the solution for $\{Y\}$ converges.

The frequency response function of $Y_j(t)$ due to the excitation $F_k(t)$, i.e., kth component of $\{F(t)\}$ follows from Eq. B-19 as

$$H_{jk}(\omega) = \frac{\phi_{kj}}{(-M_j^* \omega^2 + K_j^*) + i\omega C_j^*} \qquad \text{(B-20)}$$

Let $\{\bar{Y}(\omega)\}$ be the Fourier transform for $\{Y(t)\}$, i.e.,

$$\{\bar{Y}(\omega)\} = \int_{-\infty}^{\infty} \{Y(t)\} e^{-i\omega t} \, d\omega \qquad \text{(B-21)}$$

Then, the relationship between the Fourier transform of the derivative of a function and the Fourier transform of the function itself is

$$\{\bar{\dot{Y}}(\omega)\} = i\omega\{\bar{Y}(\omega)\} ; \quad \{\bar{\ddot{Y}}(\omega)\} = i\omega\{\bar{\dot{Y}}(\omega)\} \qquad \text{(B-22)}$$

In what follows, a quantity with a bar will indicate the Fourier transform of the quantity without a bar, without ambiguity.

The response $\{\bar{Y}(\omega)\}$ is related to the excitation $\{\bar{F}(\omega)\}$ through the transfer matrix $[H(\omega)]$,

$$[\bar{Y}(\omega)] = [H(\omega)]\{\bar{F}(\omega)\} \tag{B-23}$$

in which the element of $[H(\omega)]$ is given by Eq. B-20 and $\{\bar{F}(\omega)\}$ is the Fourier transform of $\{F(t)\}$. It follows from Eq. B-14 that

$$\{\bar{F}(\omega)\} = \left([\underline{i}\omega[\rho K_M V] + [\bar{C}]\right)\left\{\bar{\dot{V}}_0(\omega)\right\} - \left([m] + \frac{1}{\underline{i}\omega}[\bar{C}]\right)\left\{\bar{\ddot{U}}_g(\omega)\right\} \tag{B-24}$$

in which the relationship between $\left\{\bar{\dot{V}}_0(\omega)\right\}$, $\left\{\bar{\ddot{V}}_0(\omega)\right\}$, $\left\{\bar{\dot{U}}_g(\omega)\right\}$ and $\left\{\bar{\ddot{U}}_g(\omega)\right\}$ similar to that of Eq. B-22 has been used.

Substitution of Eqs. B-22 and B-24 into Eq. B-23 yields

$$\left\{\bar{\dot{Y}}(\omega)\right\} = [\Phi_V]\left\{\bar{\dot{V}}_0(\omega)\right\} + [\Phi_g]\left\{\bar{\ddot{U}}_g(\omega)\right\} \tag{B-25}$$

in which

$$\begin{aligned}[\Phi_V] &= [H(\omega)](-\omega^2[\rho K_M V] + \underline{i}\omega[\bar{C}]) \\ [\Phi_g] &= -[H(\omega)](\underline{i}\omega[m] + [\bar{C}])\end{aligned} \tag{B-26}$$

The cross-power spectral density matrix of $\{\dot{Y}(t)\}$ is by definition

$$[S_{\dot{Y}\dot{Y}}(\omega)] = \lim_{T\to\infty} \frac{1}{2\pi T} E\left[\left\{\bar{\dot{Y}}(\omega)\right\}\left\{\bar{\dot{Y}}^*(\omega)\right\}^T\right] \tag{B-27}$$

in which the star indicates the complex conjugate and T indicates the transpose of the matrix (or vector).

Using the definition of the cross-power spectral density matrix (Eq. B-27) along with Eq. B-25, one obtains

$$[S_{\dot{Y}\dot{Y}}(\omega)] = [\Phi_v][S_{\dot{v}_0\dot{v}_0}(\omega)][\Phi_v^*]^T + [\Phi_g][S_{\ddot{v}_g\ddot{v}_g}(\omega)][\Phi_g^*]^T \tag{B-28}$$

in which the cross-power spectral density matrics $[S_{\dot{v}_0\dot{v}_0}(\omega)]$ and $[S_{\ddot{u}_g\ddot{u}_g}(\omega)]$ of the wave partical velocity and the ground acceleration, respectively, are given by Eqs. 21 and 22.

The covariance matrix $[\sigma_{\dot{Y}\dot{Y}}^2]$ of the velocity vector $\{\dot{Y}(t)\}$ of the normal coordinate appearing in Eq. B-18 is obtained from the integration of the j-kth element of $[S_{\dot{Y}\dot{Y}}(\omega)]$,

$$[\sigma_{\dot{Y}\dot{Y}}^2] = \int_{-\infty}^{\infty} [S_{\dot{Y}\dot{Y}}(\omega)]d\omega \tag{B-29}$$

where $[S_{\dot{Y}\dot{Y}}(\omega)]$ is given by Eq. B-28. Note that the element $E[\dot{Y}_j\dot{Y}_k]$ appearing in Eq. B-18 is the j-kth element of $[\sigma_{\dot{Y}\dot{Y}}^2]$, i.e., $\sigma^2_{\dot{Y}_j\dot{Y}_k} = E[\dot{Y}_j\dot{Y}_k]$

The covariance matrix of the normal coordinate vector $\{Y(t)\}$, denoted by $[\sigma_{YY}^2]$, is

$$[\sigma_{YY}^2] = \int_{-\infty}^{\infty} [S_{YY}(\omega)]d\omega = \frac{1}{\omega^2}\int_{-\infty}^{\infty} [S_{\dot{Y}\dot{Y}}(\omega)]d\omega \tag{B-30}$$

where $[S_{\dot{Y}\dot{Y}}(\omega)]$ is given by Eq. B-28.

The covariance matrix of the displacement vector $\{U\}$, denoted by $[\sigma_{UU}{}^2]$, follows from Eqs. B-15 and B-30 as

$$[\sigma_{UU}{}^2] = [\phi][\sigma_{YY}{}^2][\phi]^T \tag{B-31}$$

In the iterative procedure for the vector $\{\dot{r}\}$ (see Eqs. B-11 and B-14), the quantity $\sigma_{\dot{r}_j\dot{r}_j}$ has to be estimated in order to determine $\bar{C}_{jj}$ (Eq. B-11). We first obtain $\left\{\bar{\dot{r}}(\omega)\right\}$ by taking the Fourier transform on Eq. B-12 and using Eq. B-25.

$$\begin{aligned}\left\{\bar{\dot{r}}(\omega)\right\} &= \left\{\bar{\dot{V}}_0(\omega)\right\} - [\phi]\left\{\bar{\dot{Y}}(\omega)\right\} - \left\{\bar{\ddot{U}}_g(\omega)\right\} \\ &= [\Lambda_v]\left\{\bar{\dot{V}}_0(\omega)\right\} - [\Lambda_g]\left\{\bar{\ddot{U}}_g(\omega)\right\}\end{aligned} \tag{B-32}$$

in which

$$\begin{aligned}[\Lambda_v] &= [I] - [\phi][\Phi_v] \\ [\Lambda_g] &= \frac{1}{i\omega}[I] - [\phi][\Phi_g]\end{aligned} \tag{B-33}$$

where [I] is the unit matrix, and $[\Phi_v]$ and $[\Phi_g]$ are given by Eq. B-26.

Finally, using the definition of the cross-power spectral density matrix (e.g., Eq. B-27), one obtains from Eq. B-32,

$$[S_{\dot{r}\dot{r}}(\omega)] = [\Lambda_v][S_{\dot{V}_0\dot{V}_0}(\omega)][\Lambda_v^*]^T + [\Lambda_g][S_{\ddot{U}_g\ddot{U}_g}(\omega)][\Lambda_g^*]^T \tag{B-34}$$

and hence

$$\sigma_{\dot{r}_j\dot{r}_j}^2 = \int_{-\infty}^{\infty} S_{\dot{r}_j\dot{r}_j}(\omega)\,d\omega \qquad \text{(B-35)}$$

(iii) Shear Force and Bending Moment

It follows from the equations of motion, Eq. B-13, that the shear force and the bending moment vectors, denoted by $\{Q\}$ and $\{L\}$, respectively, are given by

$$\{Q\} = [G]\{U\}$$
$$\{L\} = [R]\{U\} \qquad \text{(B-36)}$$

in which the i-jth elements of [G] and [R] are given by

$$G_{ij} = \sum_{k=1}^{i} K_{kj} \; ; \; R_{ij} = \sum_{k=1}^{i} \ell_k K_{kj} \qquad \text{(B-37)}$$

in which ℓ_k is the distance between node k-1 and node k.

From the covariance matrix of the displacement vector (U) given by Eq. B-31, it is obvious that covariance matrices of (Q) and (L) are

$$[\sigma_{QQ}^2] = [G][\phi][\sigma_{YY}^2][\phi]^T[G]^T$$
$$[\sigma_{LL}^2] = [R][\phi][\sigma_{YY}^2][\phi]^T[R]^T \qquad \text{(B-38)}$$

where $[\sigma_{YY}^2]$ are given by Eq. B-30.

TABLE 1 : STRUCTURAL PROPERTY FOR 1075' TOWER

NODES	Y	M	V	A
1	-75	330	0	0
2	10	101	28750	14643
3	75	146	46875	19429
4	205	383	117750	33500
5	400	537	189250	46286
6	600	665	245250	49857
7	800	1191	448750	63071

Total Weight G = 107,966.6 kips

First Three Natural Frequencies (rad/sec) 1.155 , 2.201 , 3.663

Flexibility Matrix $[k]^{-1}$ (10^{-6} ft/kip)

756	622	531	374	210	98.2	30.8
	568	491	357	209	102	33.6
		464	344	207	105	35.8
			321	205	110	40.1
Symmetric				203	118	46.5
					126	53.2
						58.8

TABLE 2 : STRUCTURAL PROPERTY FOR 675' TOWER

NODES	Y	M	V	A
1	-75	330	0	0
2	10	101	29950	11929
3	75	89.2	28650	10071
4	140	165	59600	16500
5	270	292	103250	24000
6	400	369	135250	26000
7	530	417	163000	31286

Total Weight G = 56,775 kips

First Three Natural Frequencies (rad/sec.): 1.851 , 3.958 , 7.273

Flexibility Matrix $[k]^{-1}(10^{-6}$ ft/kip)

455	346	274	211	111	49.2	9.4
	314	253	199	112	52	10.6
		240	191	112	54.1	11.4
Symmetric			186	112	56.2	12.3
				115	60.2	14.1
					65.2	15.8
						16.6

TABLE 3 : STRUCTURAL PROPERTIES FOR 475' TOWER

NODES	Y	M	V	A
1	-75	330	0	0
2	10	101	29850	11786
3	75	89.2	28650	10071
4	140	105	33200	10714
5	205	126	43900	11286
6	270	151	53950	12357
7	335	256	118750	23214

Total Weight G = 37,294 kips

First Three Natural Frequencies (rad/sec): 2.593 , 6.074 , 10.55

Flexibility Matrix $[k]^{-1}(10^{-6}$ ft/kip)

288	207	149	101	60	29.8	9.4
	189	140	97.5	61.5	32.3	11.3
		136	96	62	34.7	12.7
			97	64	36.8	14.1
Symmetric				67.5	40.3	15.4
					43.9	18.0
						18.3

TABLE 4 : STANDARD DEVIATIONS OF BASE SHEAR FORCES IN KIPS; (RETURN PERIOD 12.5 YEARS)

1075' TOWER			
Nonlinear Solution		Linear Solution	
Storm Waves W = 120 ft/sec	Earthquakes $S=0.1031\ ft/sec^2\ rad^{1/2}$	Storm Waves W =120 ft/sec	Earthquakes $S=0.1031\ ft/sec^2\ rad^{1/2}$
5950	2125	2900	2630

475' Tower			
Nonlinear Solution		Linear Solution	
Storm Waves W = 120 ft/sec	Earthquakes $S=0.1031\ ft/sec^2 rad^{1/2}$	Storm Waves W = 120 ft/sec	Earthquakes $S=0.1031\ ft/sec^2 rad^{1/2}$
3680	1165	1430	1244

Figure Captions

Fig. 1 : Environmental Loads; Storm Waves $X_1(t)$, Earthquakes $X_2(t)$, and Joint Occurrences $X_3(t)$.

Fig. 2 : Lumped Mass Model of an offshore tower.

Fig. 3 : Relationship between the expected maximum wave height Y_{1m} and the average storm wind velocity W at 64' above the sea surface.

Fig. 4 : Distribution functions of the expected maximum wave height; (a) the Gulf of Alaska, (b) the Northern North Sea, (c) the Gulf of Mexico, (d) the Mustang Island.

Fig. 5 : Probability density functions of the average storm wind velocity $f_W(y)$; (a) the Gulf of Alaska, (b) the Northern North Sea, (c) the Gulf of Mexico, (d) the Mustang Isalnd.

Fig. 6 : Relationship between the expected maximum ground acceleration Y_{2m} and the earthquake intensity S.

Fig. 7 : Distribution functions of the expected maximum ground motion in the Gulf of Alaska (from Ref. 2); (a) Expected Maximum Ground Acceleration, (b) Expected Maximum Ground Velocity.

Fig. 8 : Probability Density Function of Earthquakes Intensity, S, in the Gulf of Alaska.

Fig. 9 : Standard Deviations of Responses vs. Average Storm Wind Velocity W at 64' above the Sea surface, (a) Base Shear, (b) Base Moment

Fig. 10 : Standard Deviations of Response vs. Earthquake Intensity S, (a) Base Shear, (b) base moment

Fig. 11 : Exceedance curves per storm; (a) 1075' tower (b) 475' tower.

Fig. 12 : Exceedance curves per earthquake; (a) 1075' tower (b) 475' tower.

Fig. 13 : Probability of failure per storm for various average storm wind velocity and design characteristic strength β (in term of G); (a) 1075' tower, (b) 675' tower, (c) 475' tower.

Fig. 14 : Probability of failure per earthquake for various earthquake intensity and design characteristic strength β (in term of G); (a) 1075' tower, (b) 475' tower.

Fig. 15 : Probabilities of failure per occurrence of (i) storm waves p_1, (ii) Earthquake p_2, and (iii) both storm waves and earthquakes p_3, for various design characteristic strength β in the Gulf of Alaska; (a) 1075 ft. tower, (b) 675 ft. tower, (c) 475 ft. tower.

Fig. 16 : Probabilities of failure per Storm waves, p_1, vs. the design strength β at various geological locations; (a) 1075 ft. tower, (b) 675 ft. tower, (c) 475 ft. tower.

Fig. 17 : Probabilities of failure vs. service time t in the Gulf of Alaska; (a) 1075 ft. tower, (b) 475 ft. tower.

Fig. 18 : Probabilities of failure (and reliability) in 25 years of service vs. design strength β; (a) 1075' tower, (b) 675' tower, (c) 475' tower.

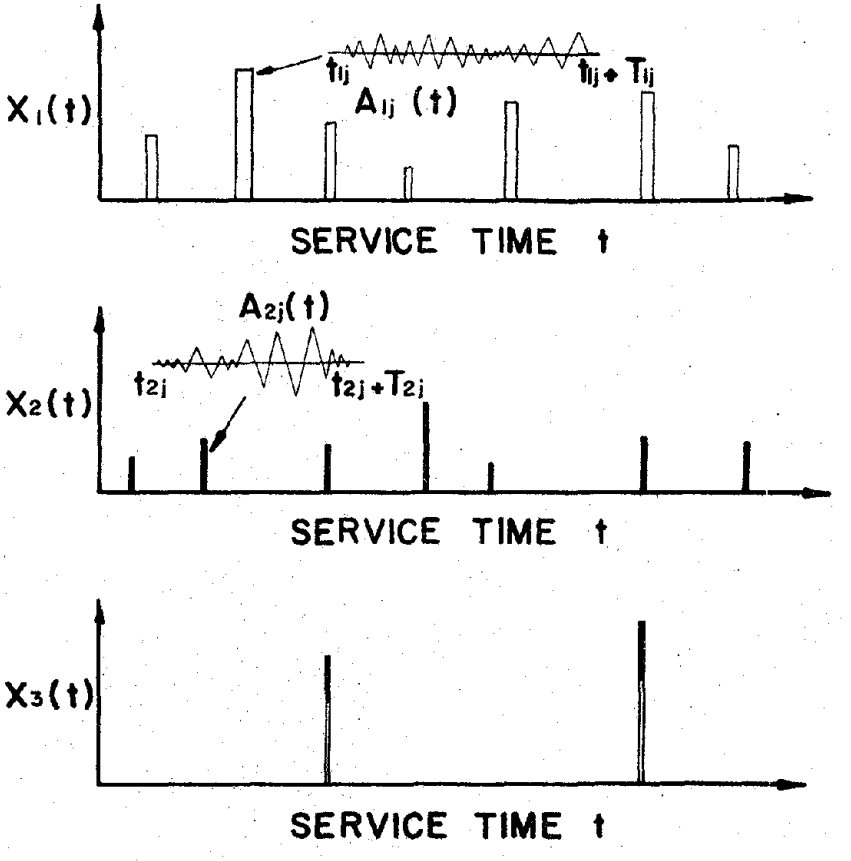

Fig. 1: Environmental Loads; Storm Waves $X_1(t)$, Earthquakes $X_2(t)$, and Joint Occurrences $X_3(t)$.

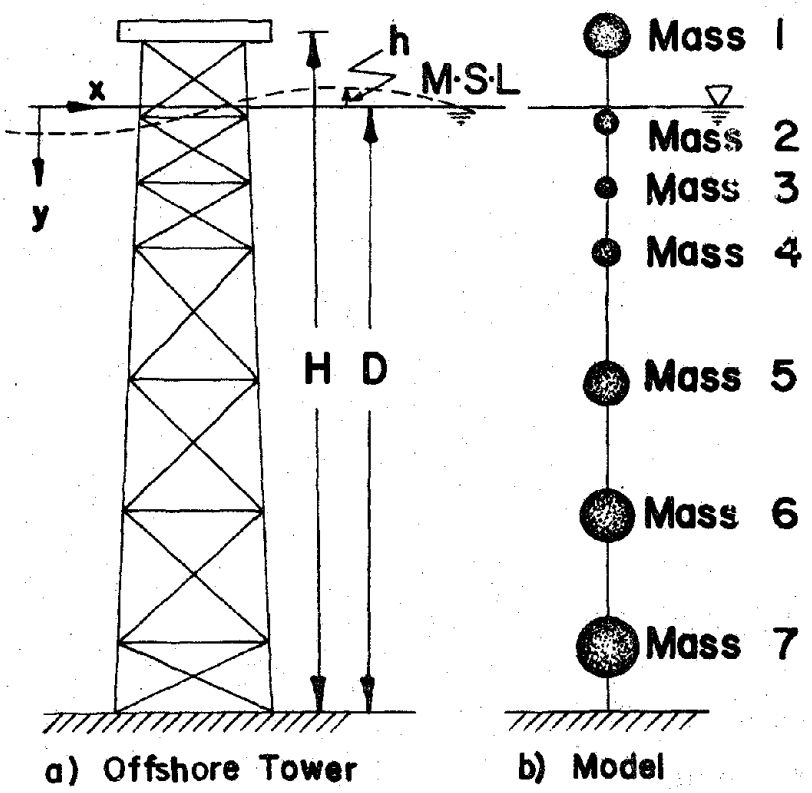

Fig. 2: Lumped Mass Model of an offshore tower.

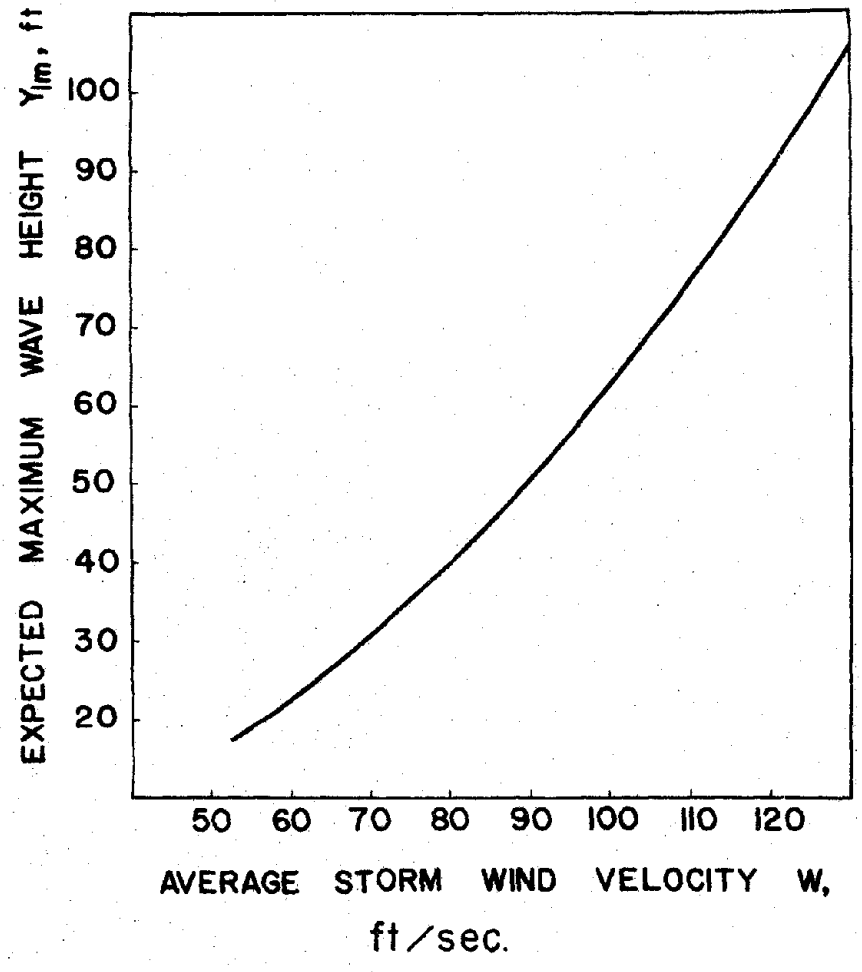

Fig. 3: Relationship between the expected maximum wave height Y_{1m} and the average storm wind velocity W at 64' above the sea surface.

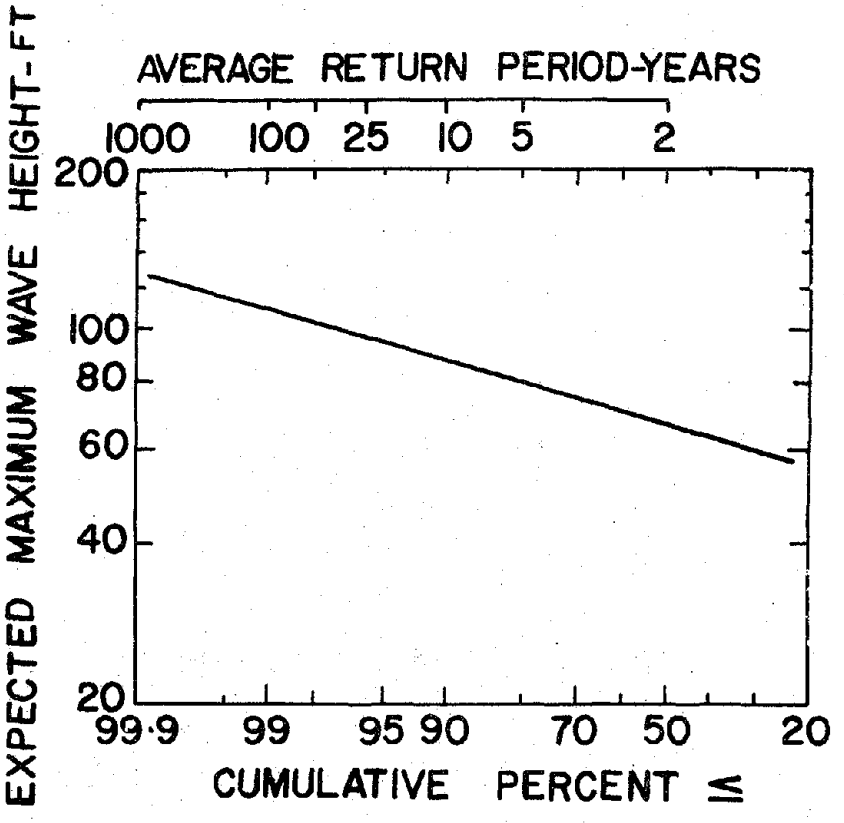

Fig. 4(a): Gulf of Alaska

Fig. 4: Distribution functions of the expected maximum wave height; (a) the Gulf of Alaska, (b) the Northern North Sea, (c) the Gulf of Mexico, (d) the Mustang Island.

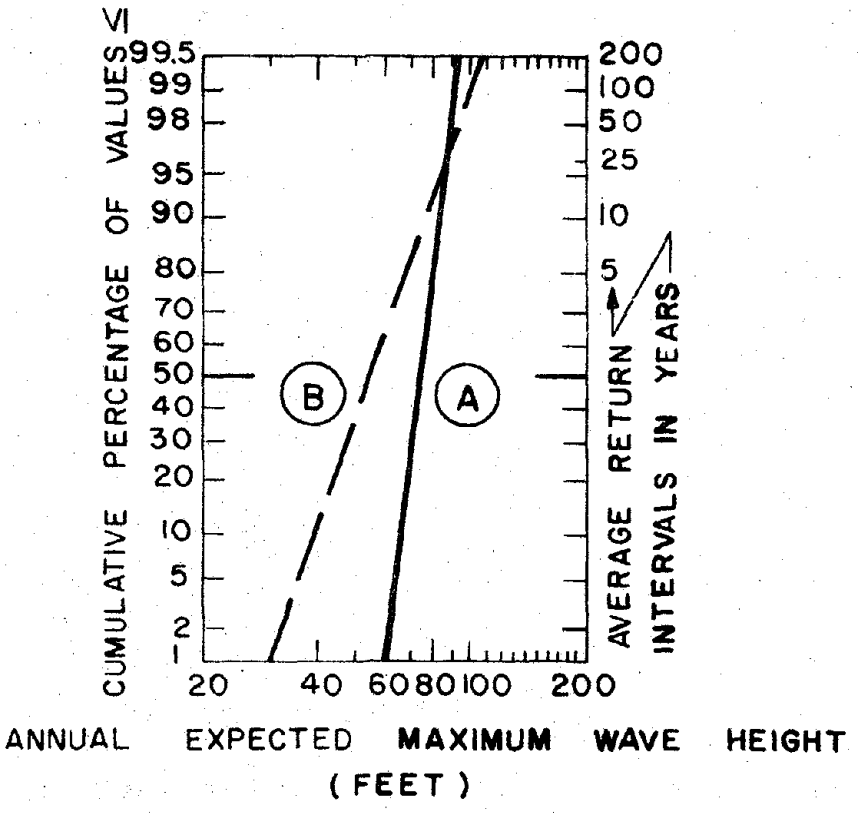

Fig. 4(b): Northern North Sea

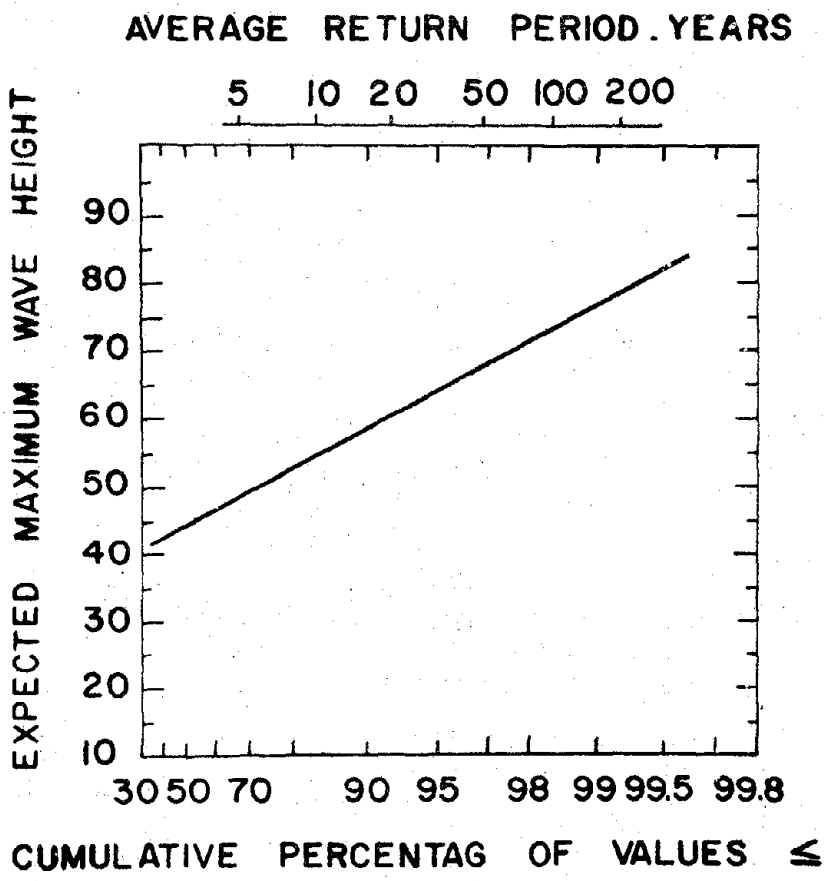

Fig. 4(c): Gulf of Mexico

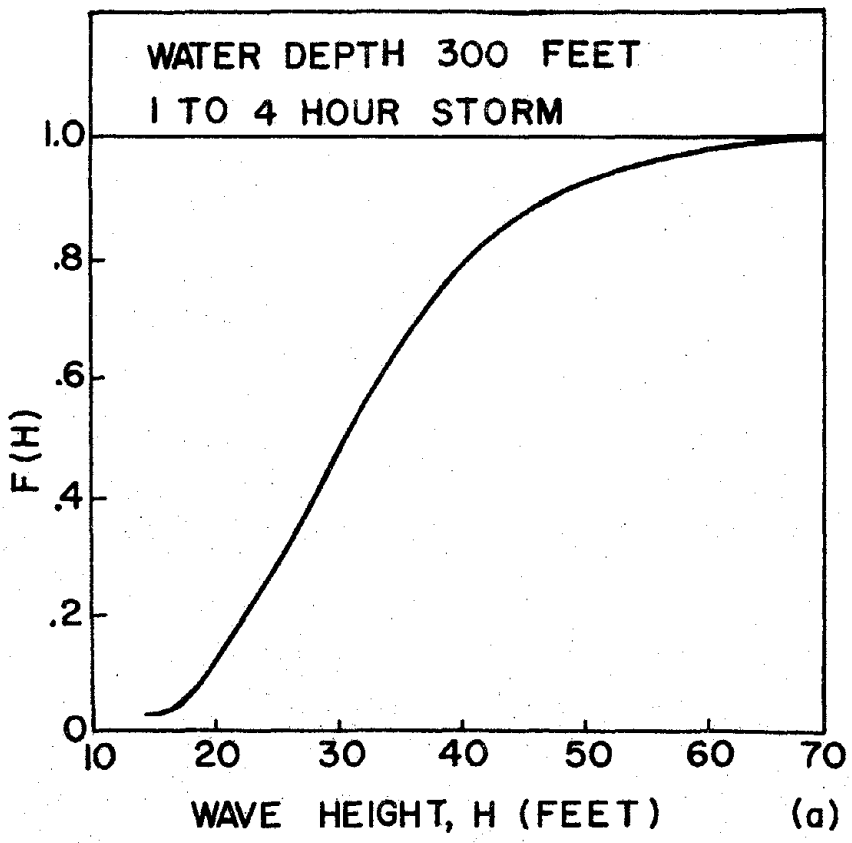

Fig. 4(d): Mustang Island

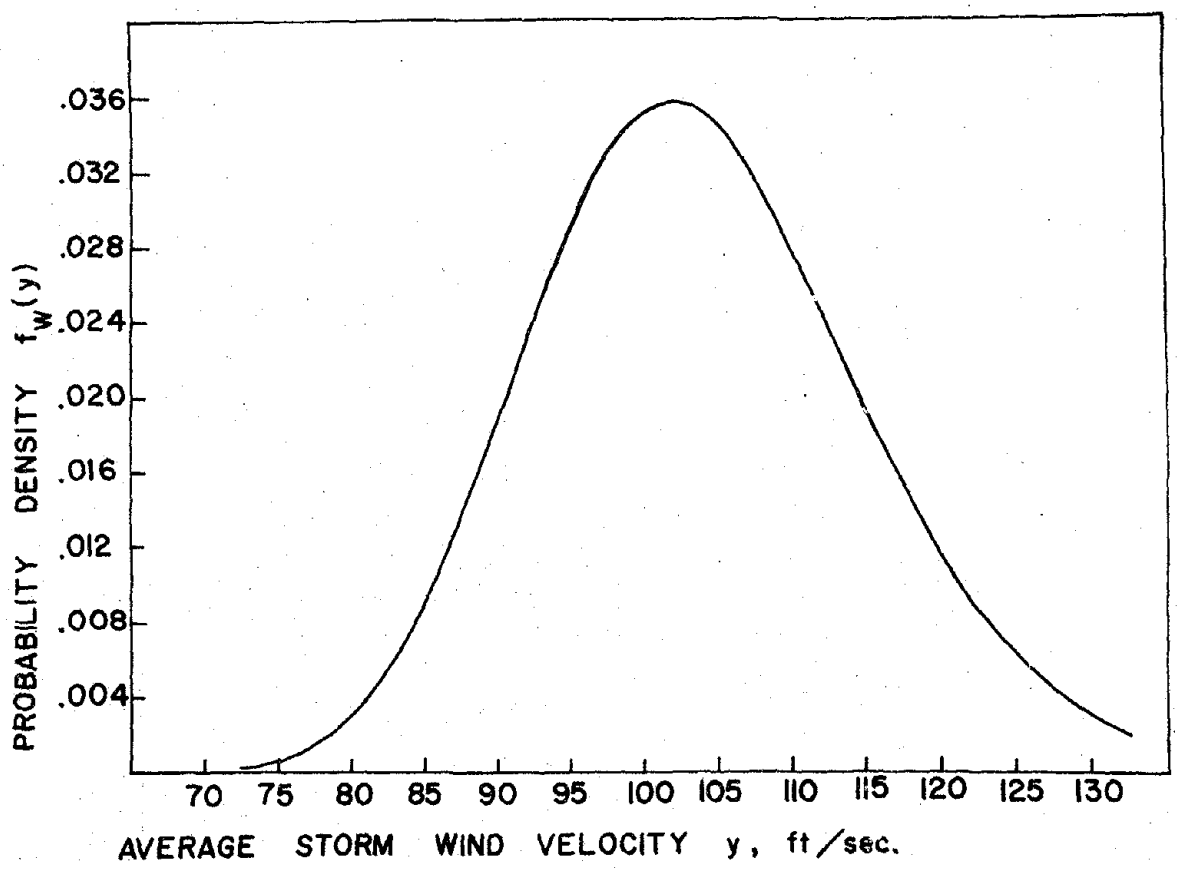

Fig. 5(a): Gulf of Alaska

Fig. 5: Probability density functions of the average wind velocity $f_W(y)$; (a) the Gulf of Alaska, (b) the Northern North Sea, (c) the Gulf of Mexico, (d) the Mustang Island.

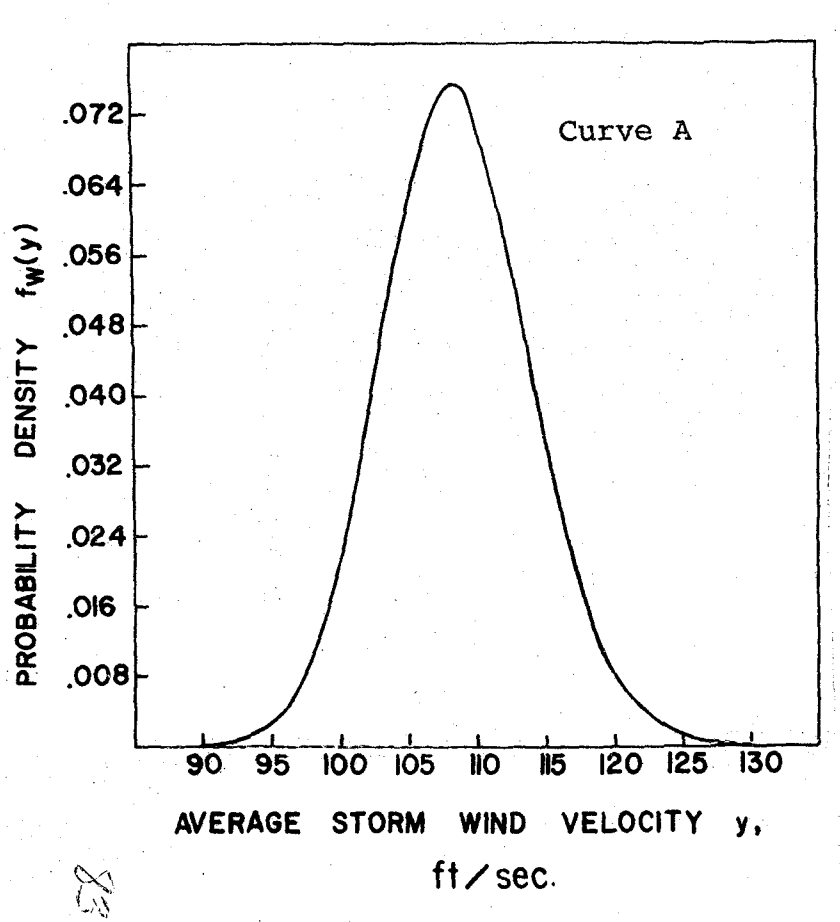

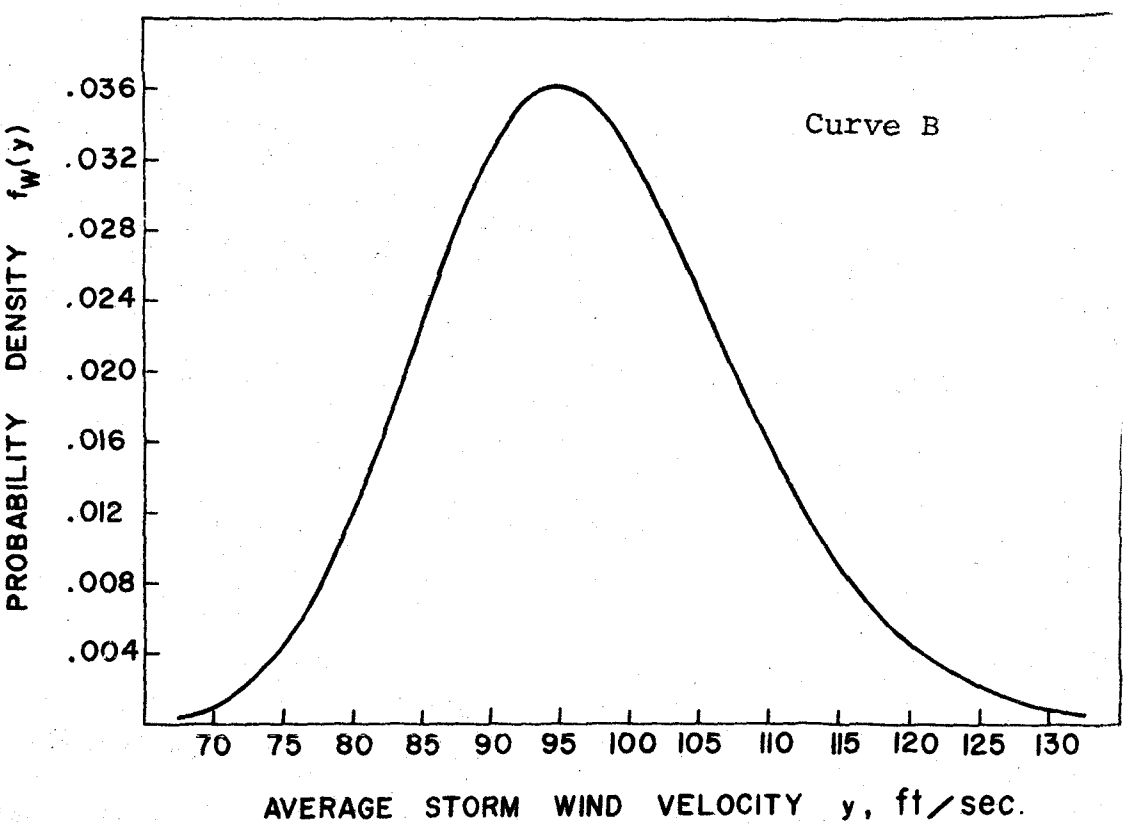

Fig. 5(b): Northern North Sea

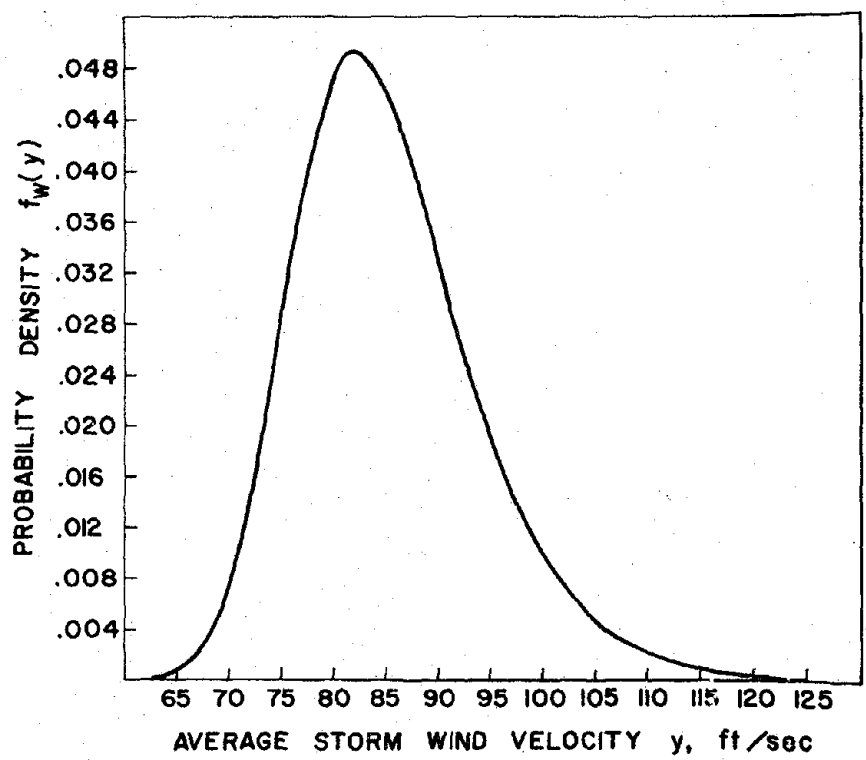

Fig. 5(c): Gulf of Mexico

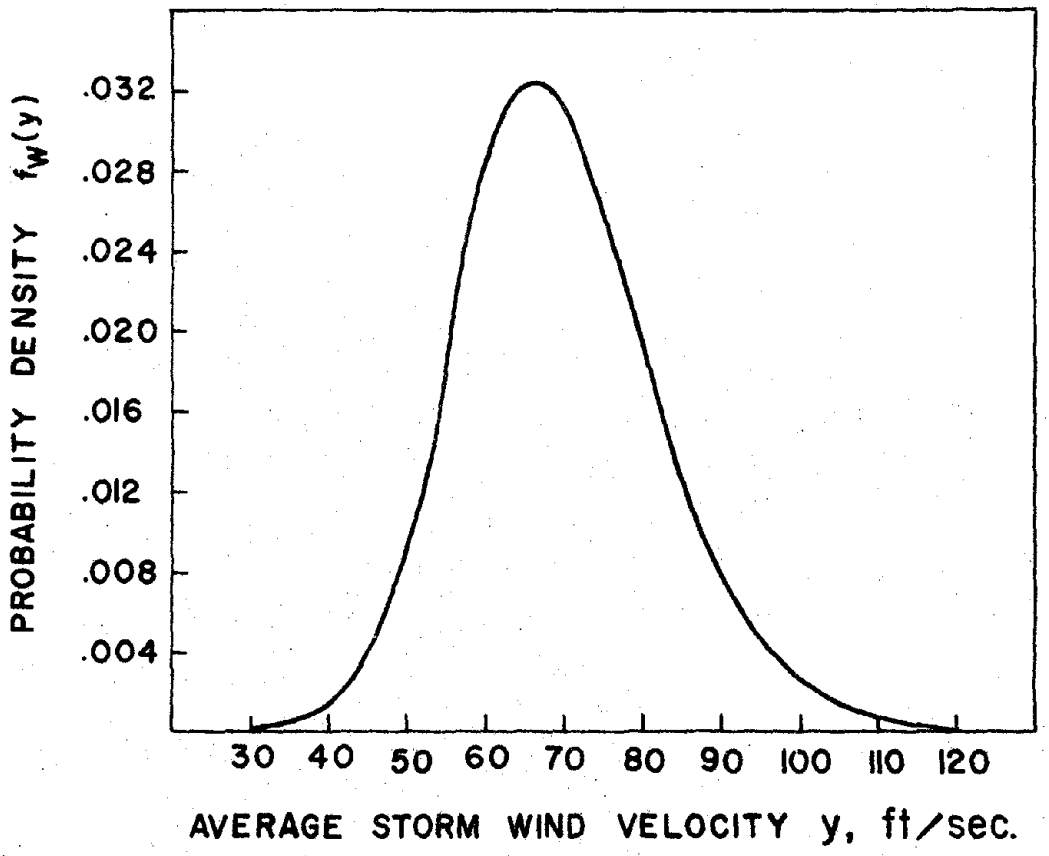

Fig. 5(d): Mustang Island

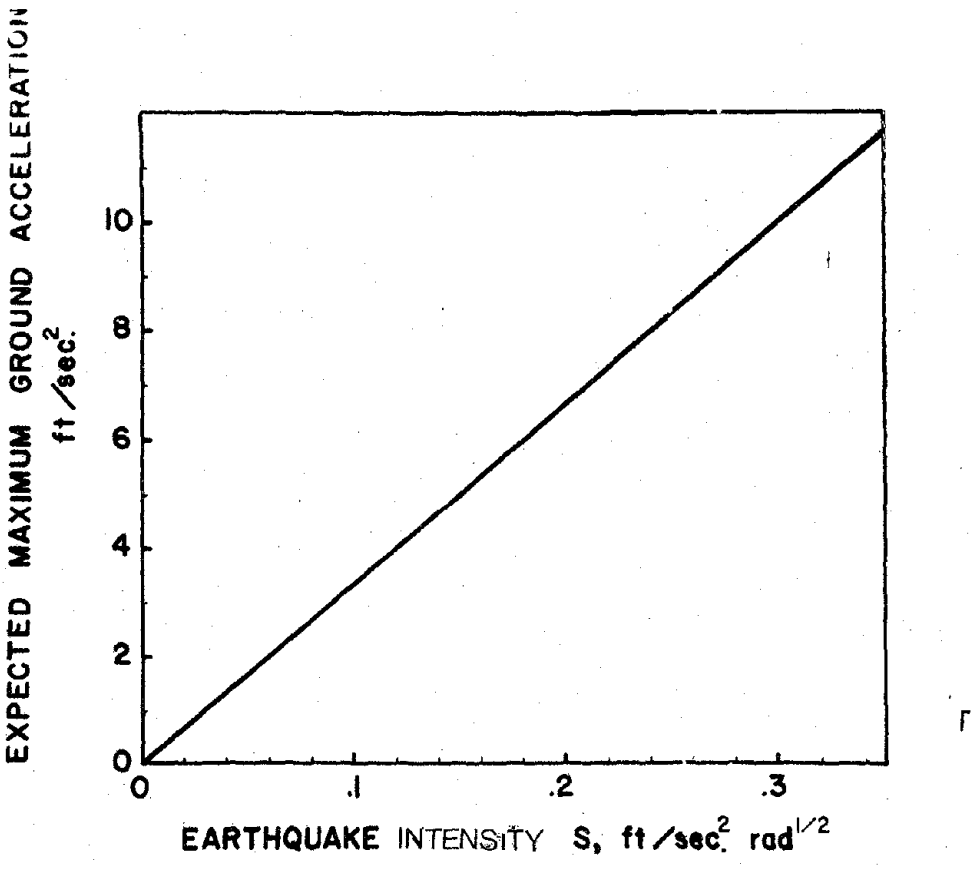

Fig. 6: Relationship between the expected maximum ground acceleration Y_{2m} and the earthquake intensity S.

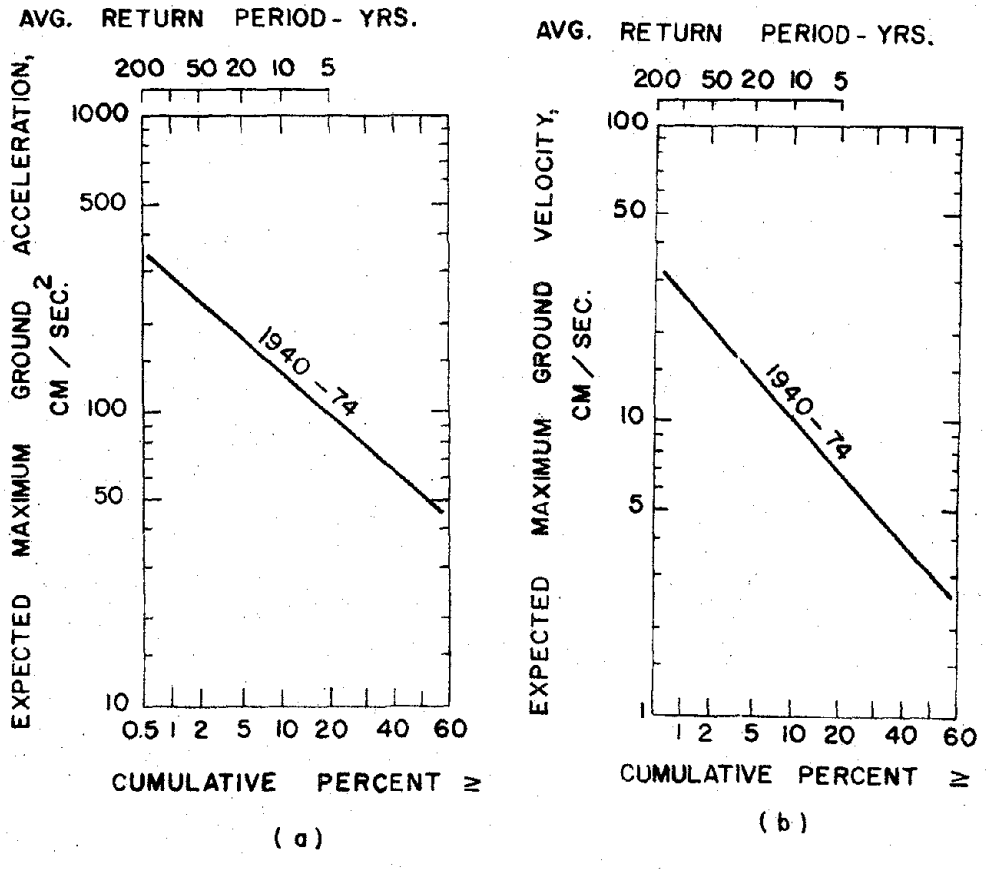

Fig. 7: Distribution functions of the expected maximum ground motion in the Gulf of Alaska (from Ref. 2); (a) Expected Maximum Ground Acceleration, (b) Expected Maximum Ground Velocity.

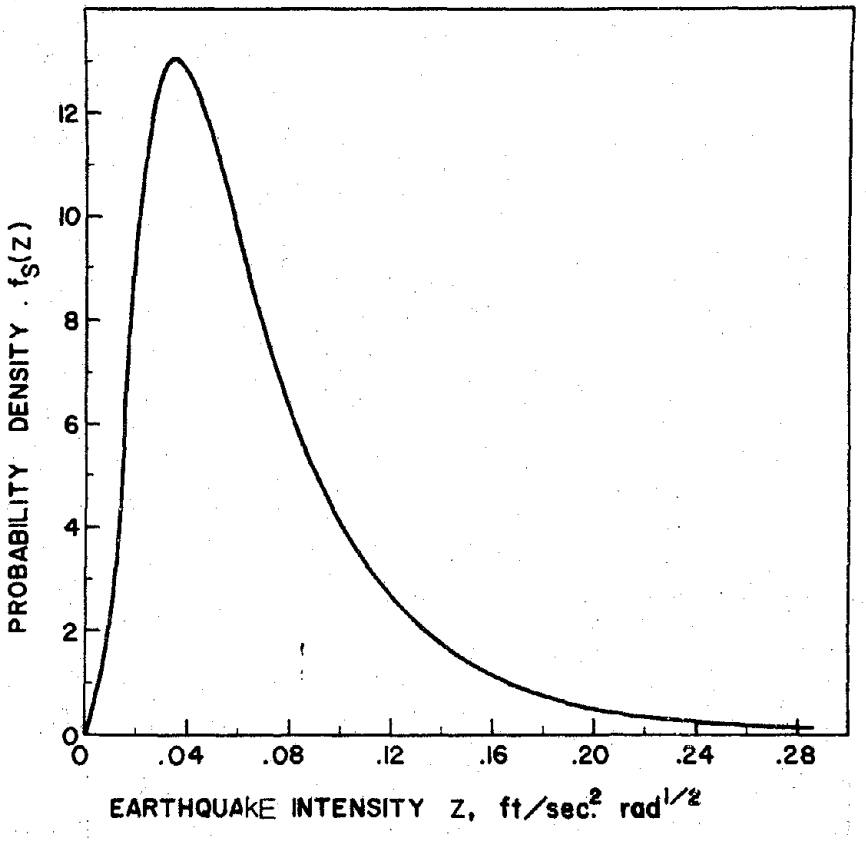

Fig. 8: Probability Density Function of Earthquake Intensity, S, in the Gulf of Alaska.

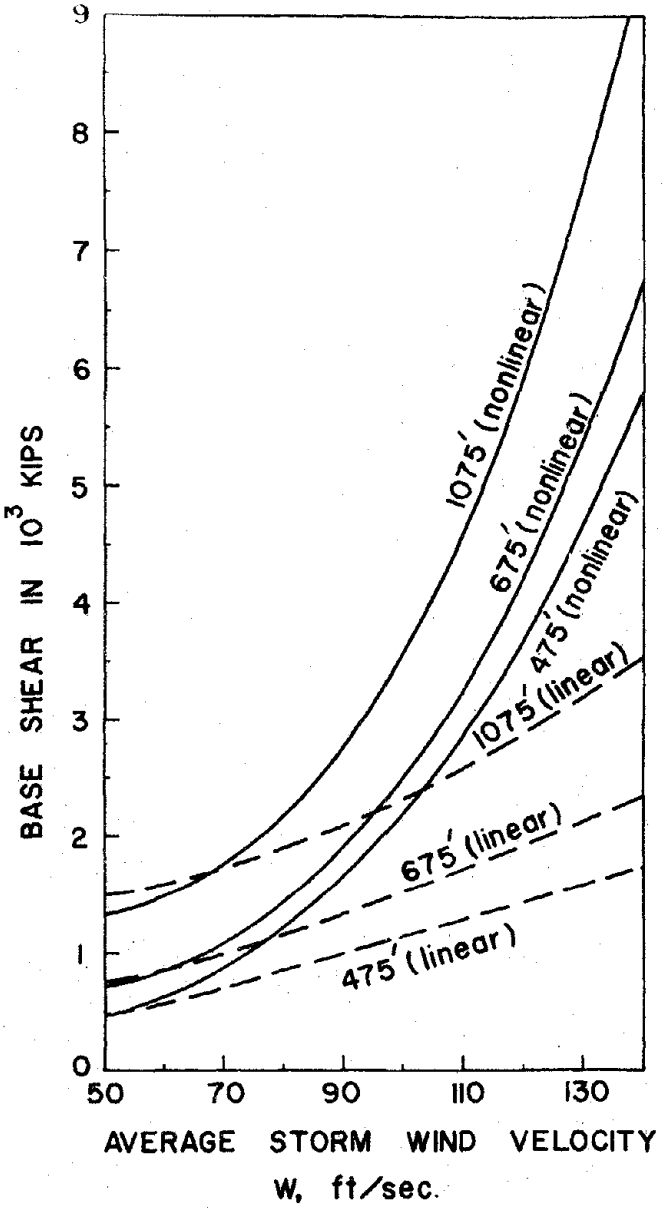

Fig. 9(a): Base Shear Force

Fig. 9: Standard Deviations of Responses vs. Average Storm Wind Velocity W at 64' above the Sea Surface, (a) Base Shear, (b) Base Moment.

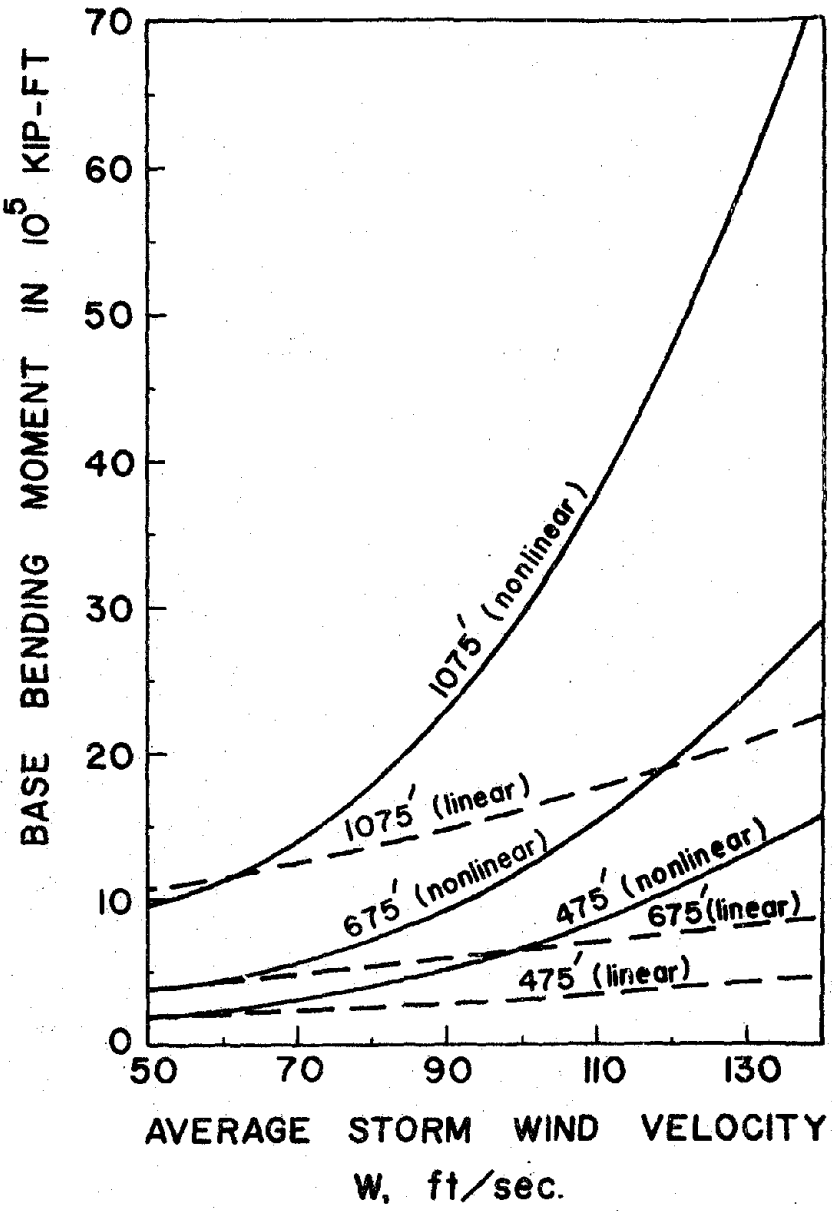

Fig. 9(b): Base Moment

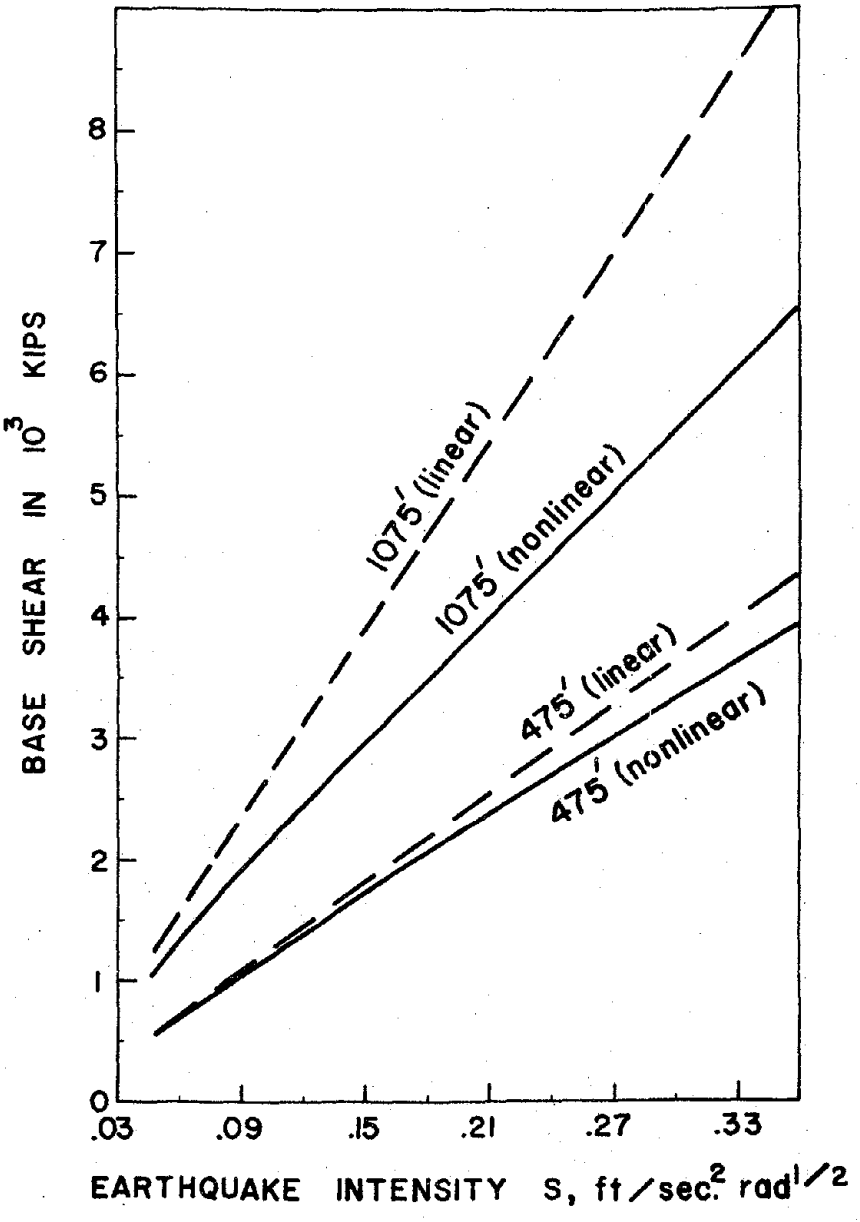

Fig. 10(a): Base Shear Force

Fig. 10: Standard Deviations of Responses vs. Earthquake Intensity S, (a) Base Shear, (b) Base Moment.

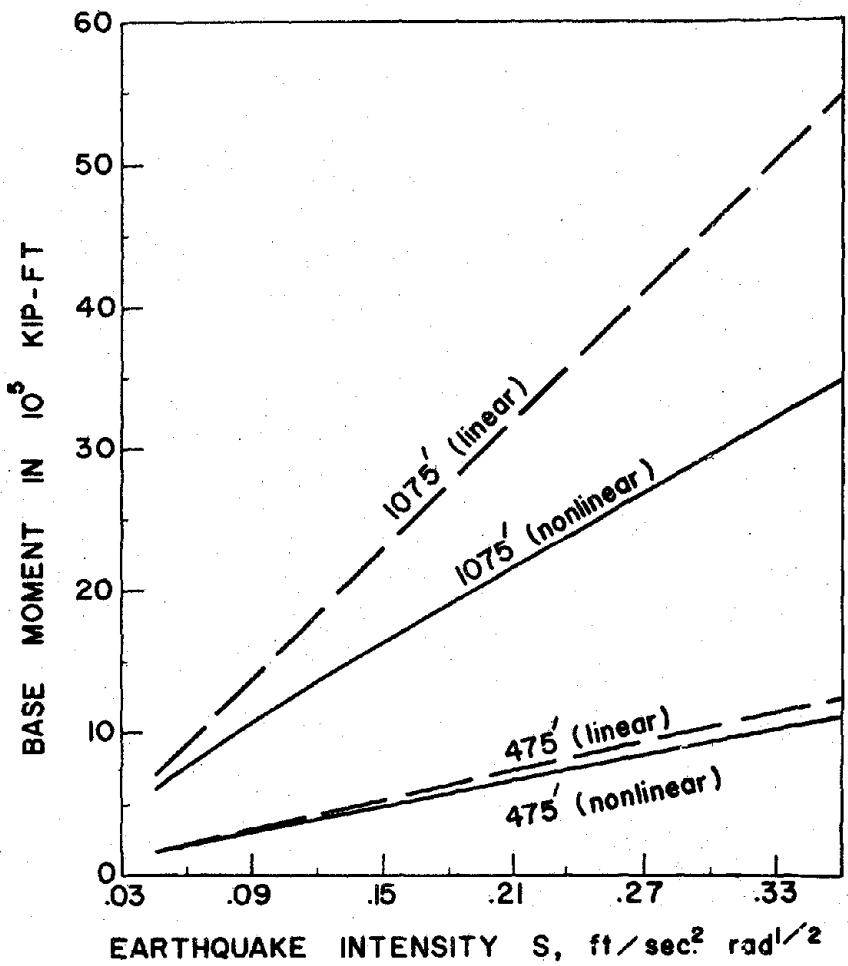

Fig. 10(b): Base Moment

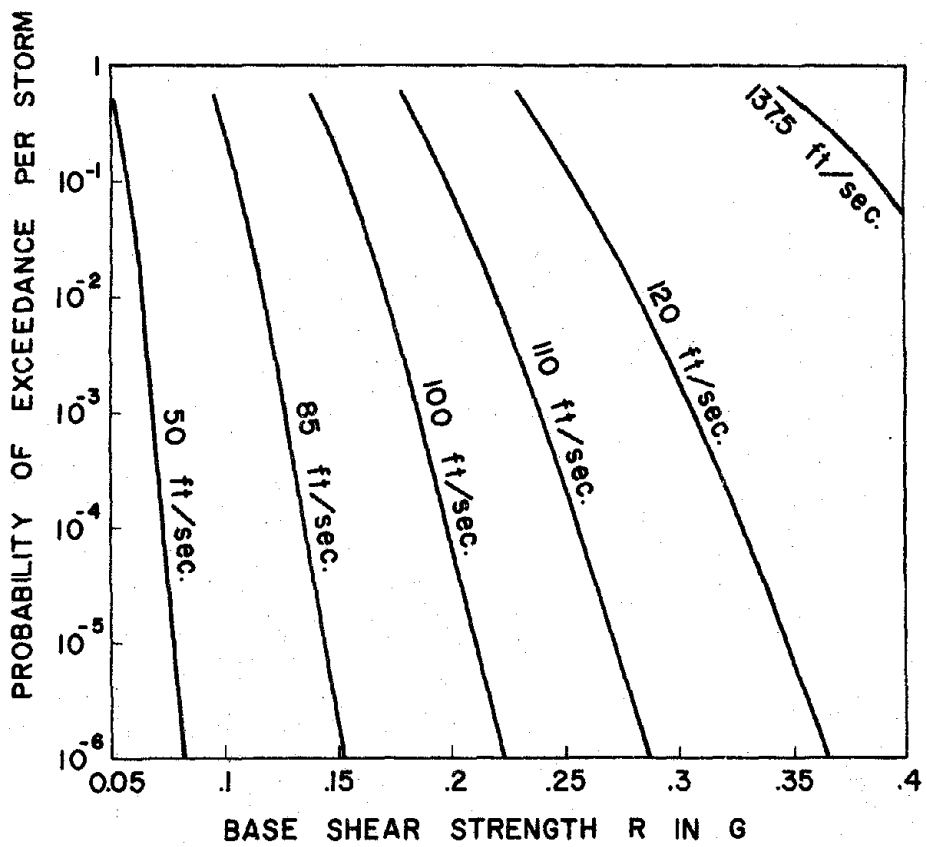

Fig. 11(a): 1075' Tower

Fig. 11: Exceedance curves per storm; (a) 1075' tower, (b) 475' tower.

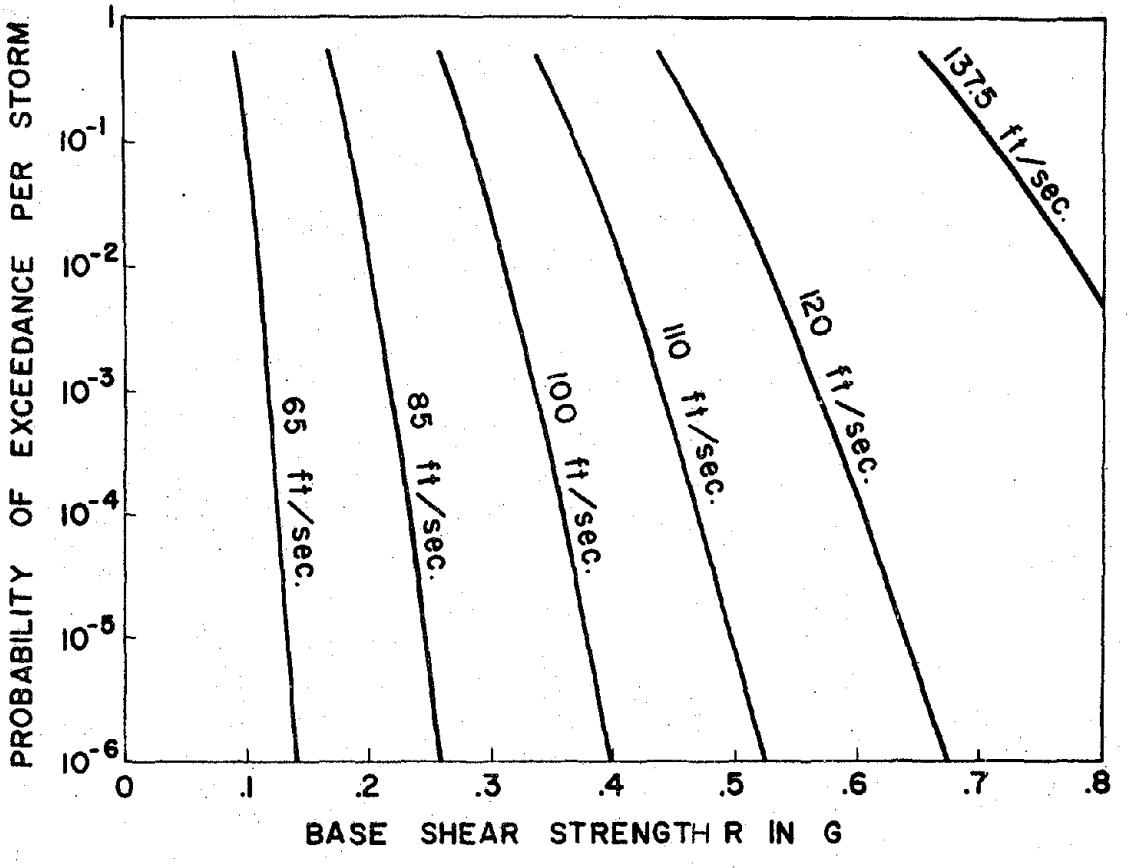

Fig. 11(b): 425' Tower

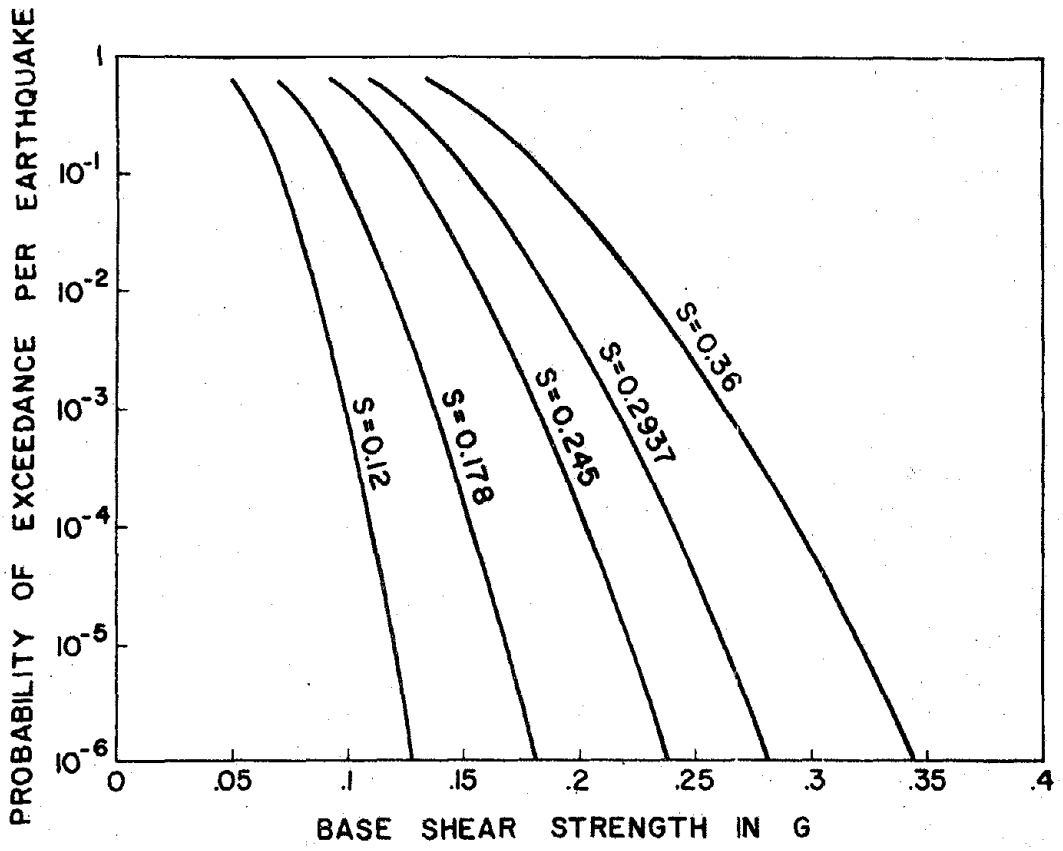

Fig. 12(a): 1075' Tower

Fig. 12: Exceedance curves per earthquake; (a) 1075' tower, (b) 475' tower.

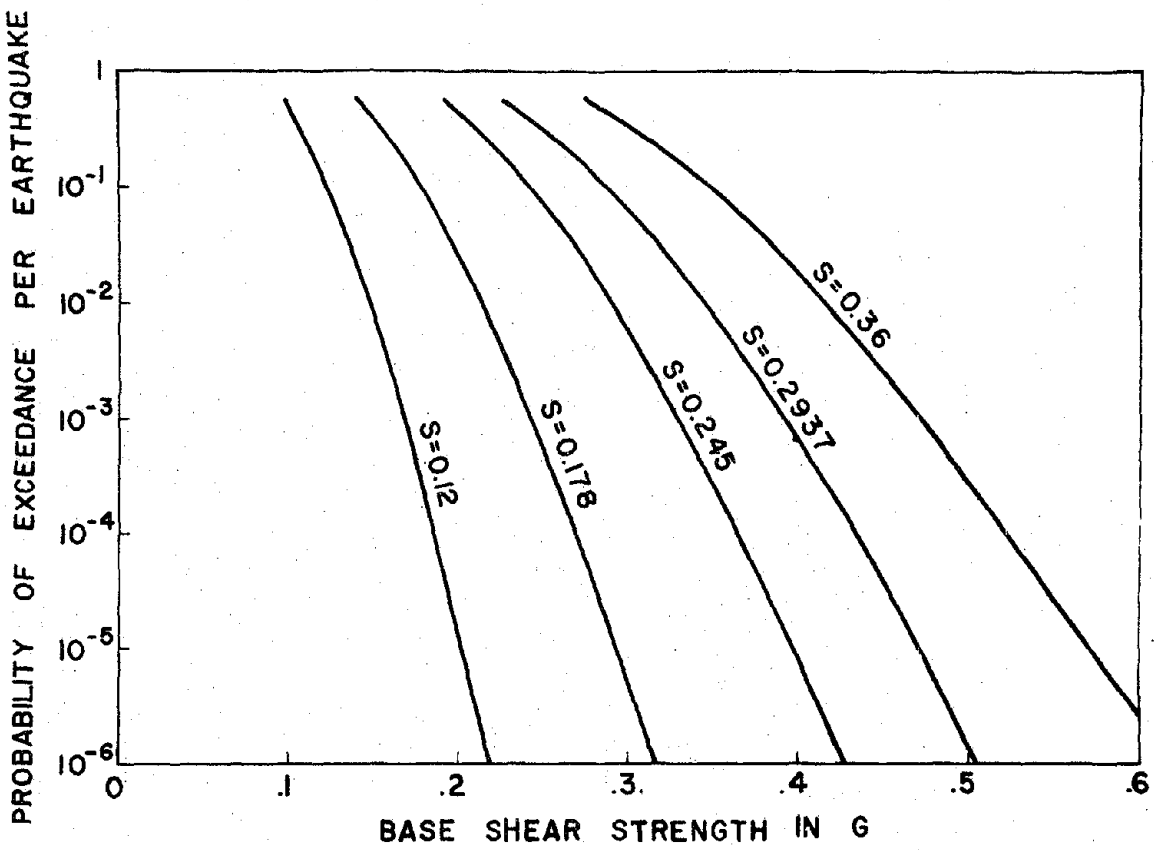

Fig. 12(b): 425' Tower

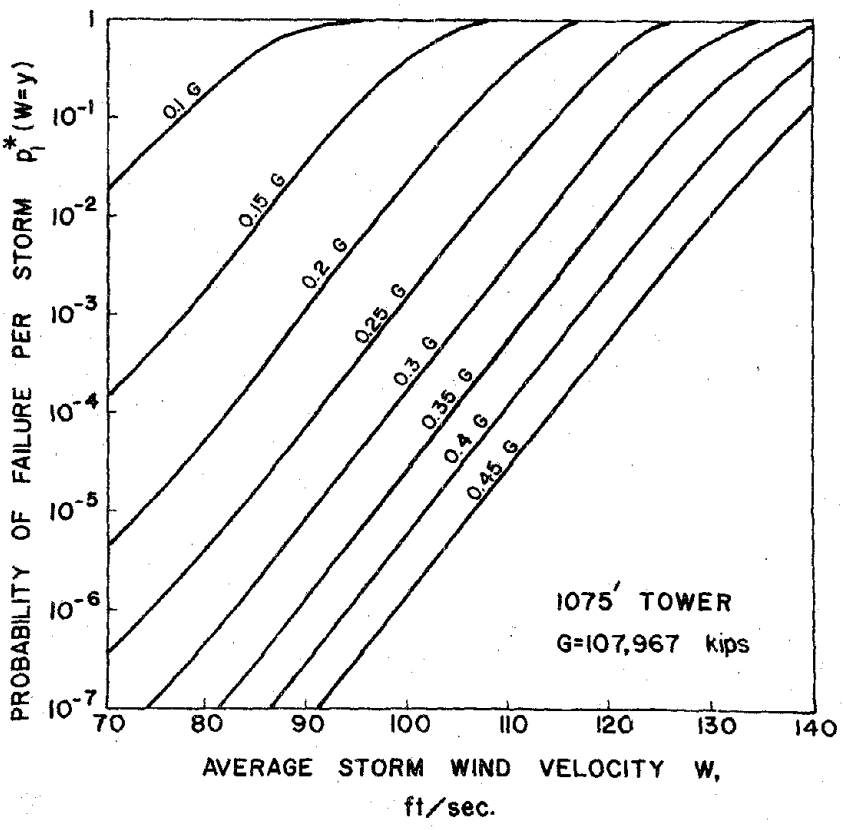

Fig. 13(a): 1075' Tower

Fig. 13: Probability of failure per storm for various average storm wind velocity and design characteristic strength β (in term of G); (a) 1075' tower, (b) 675' tower, (c) 475' tower.

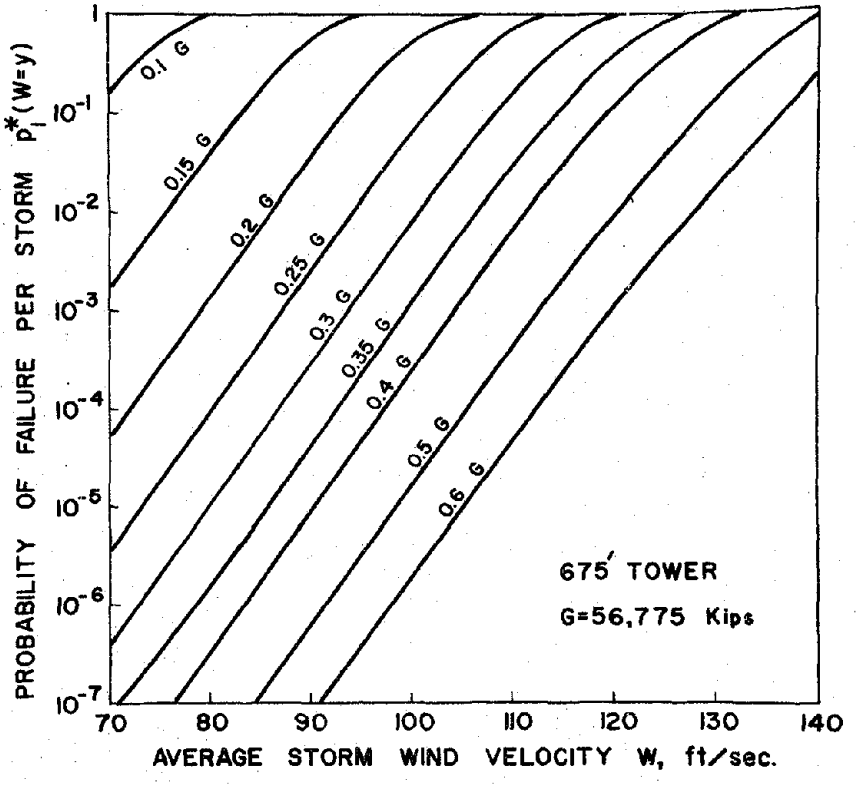

Fig. 13(b): 675' Tower

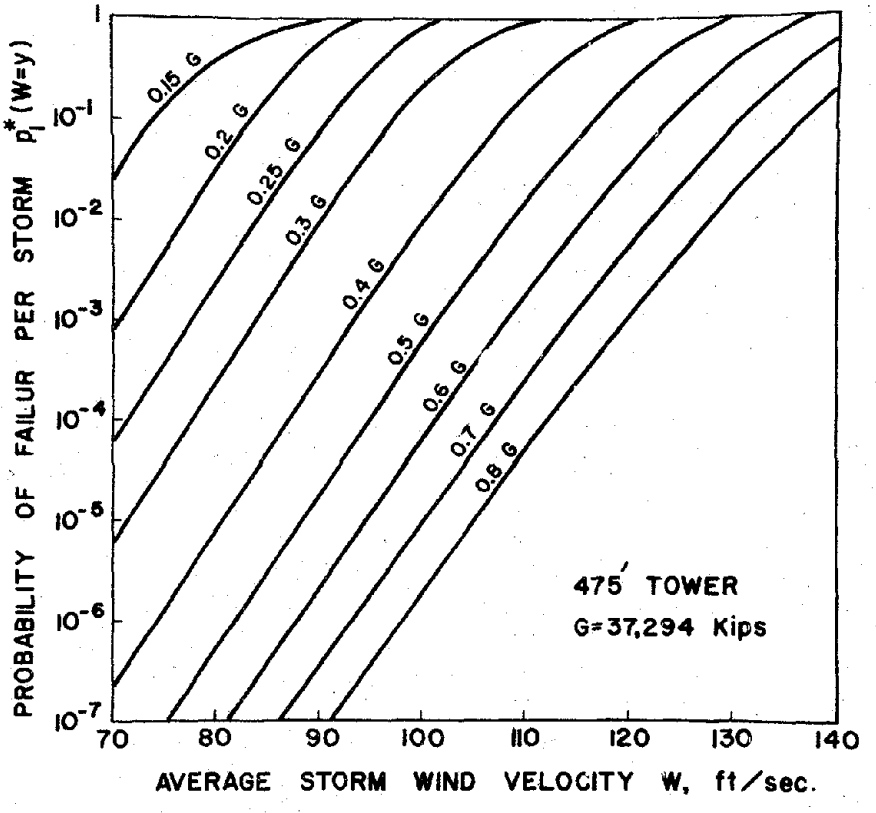

Fig. 13(c): 475' Tower

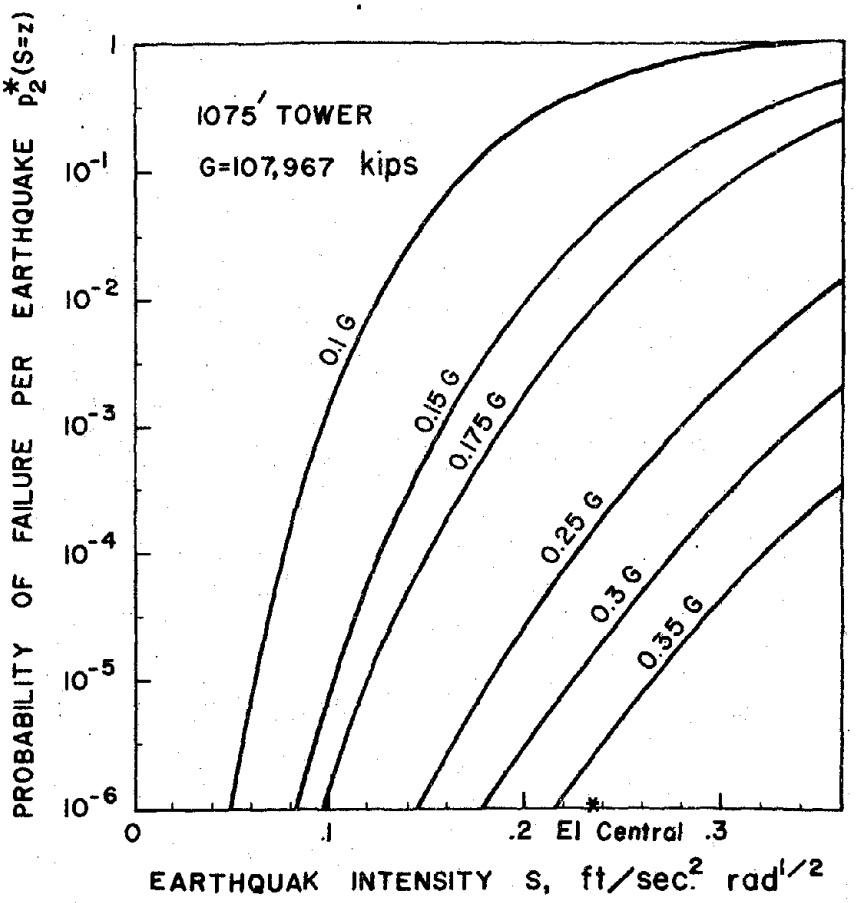

Fig. 14(a): 1075' Tower

Fig. 14: Probability of failure per earthquake for various earthquake intensity and design characteristic strength β(in term of G); (a) 1075' tower, (b) 475' tower.

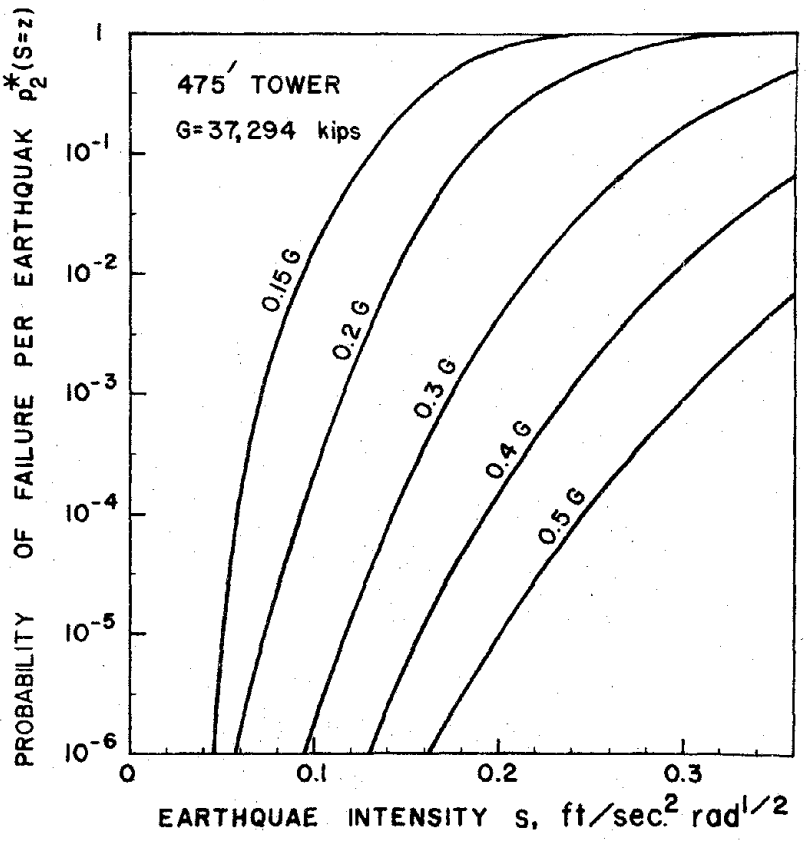

Fig. 14(b): 475' Tower

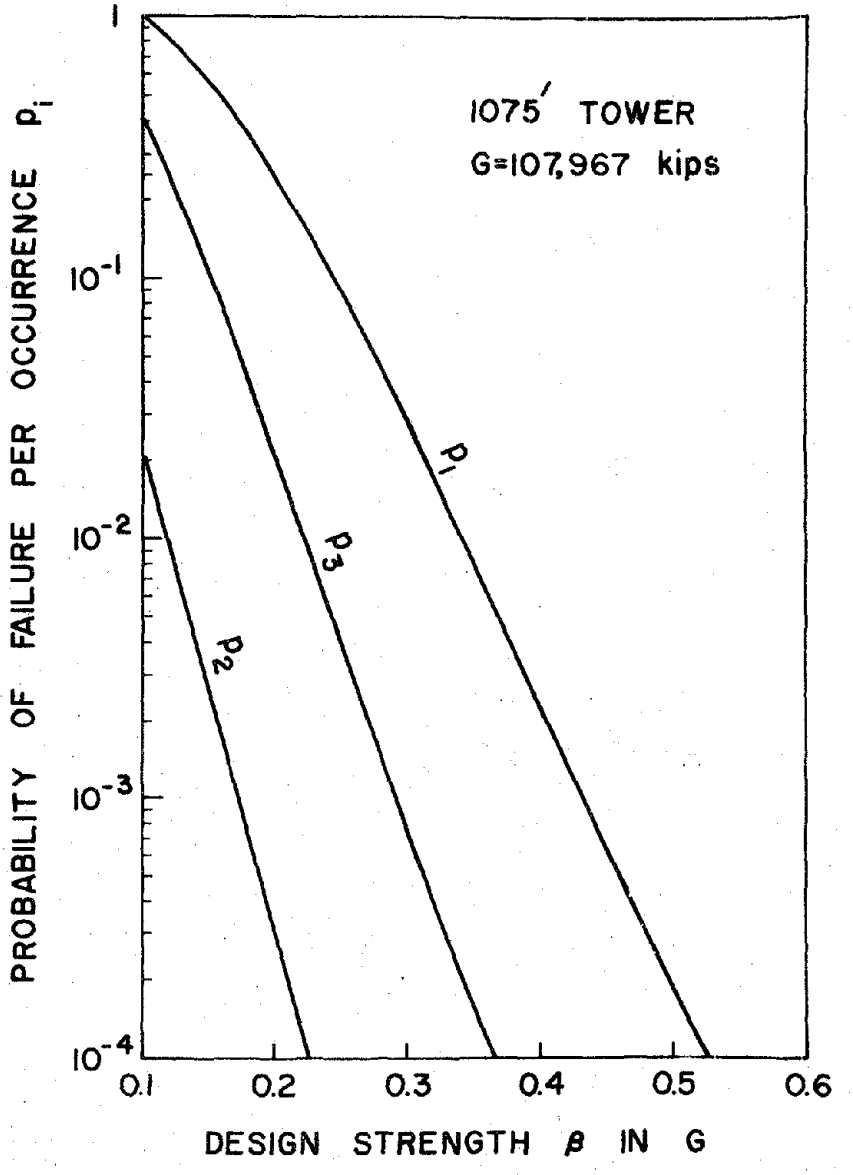

Fig. 15(a): 1075' Tower

Fig. 15: Probabilities of failure per occurrence of (i) storm waves p_1, (ii) Earthquake p_2, and (iii) both storm waves and earthquakes p_3, for various design characteristic strength β in the Gulf of Alaska; (a) 1075' tower, (b) 675' tower, (c) 475' tower.

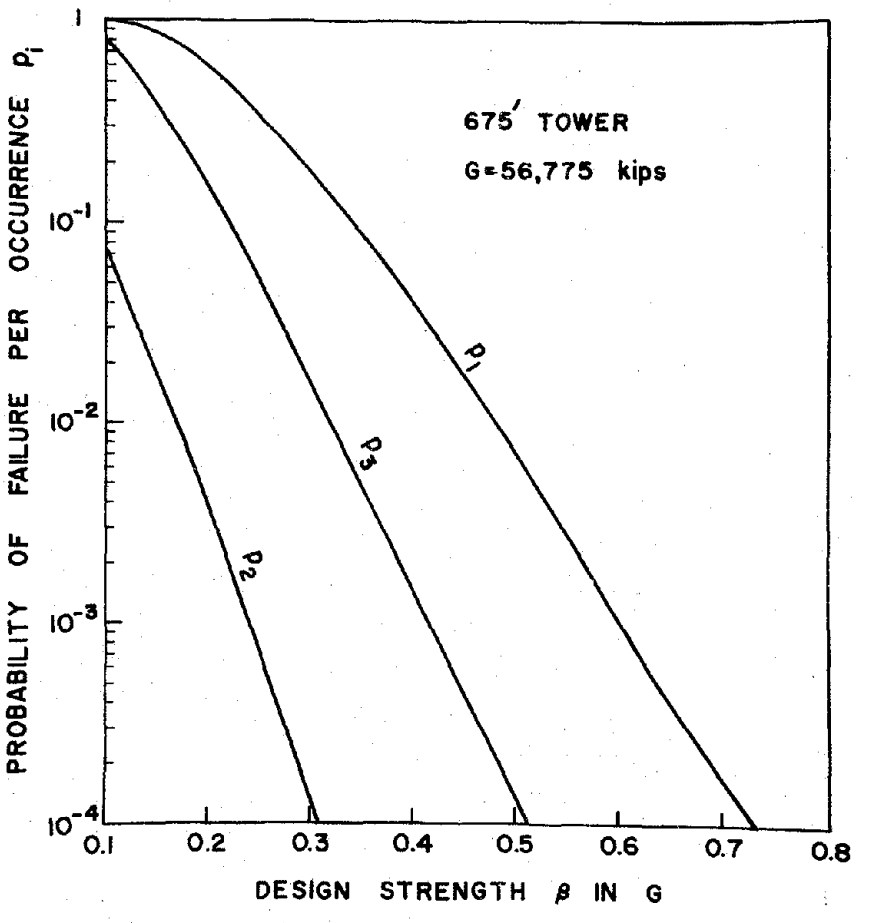

Fig. 15(b): 675' Tower

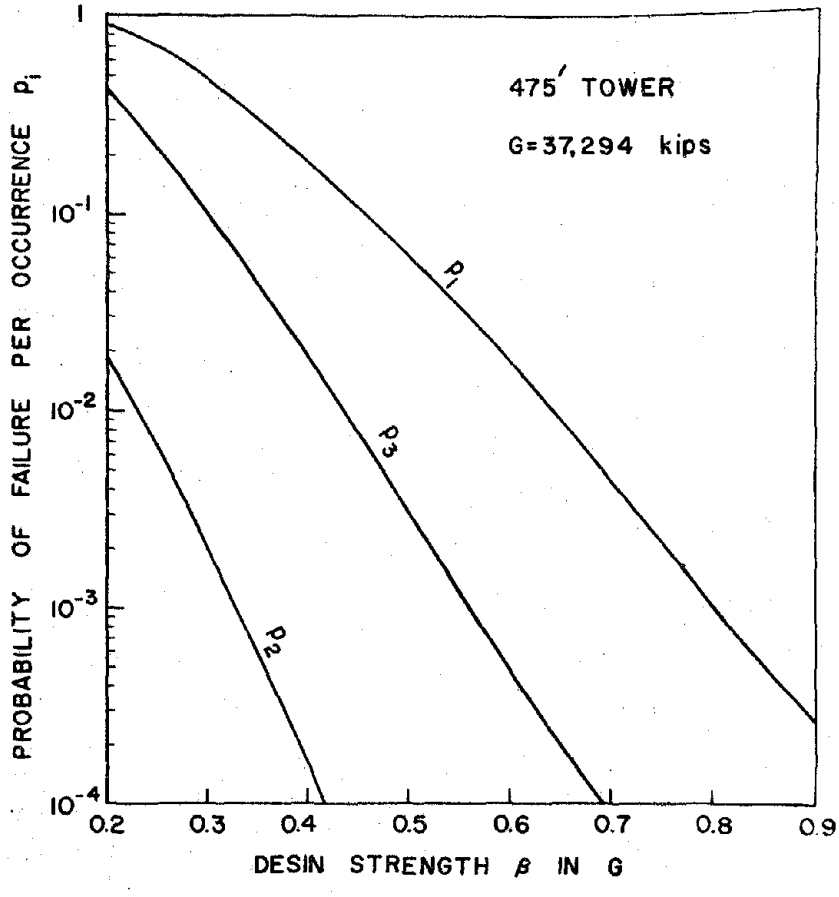

Fig. 15(c): 475' Tower

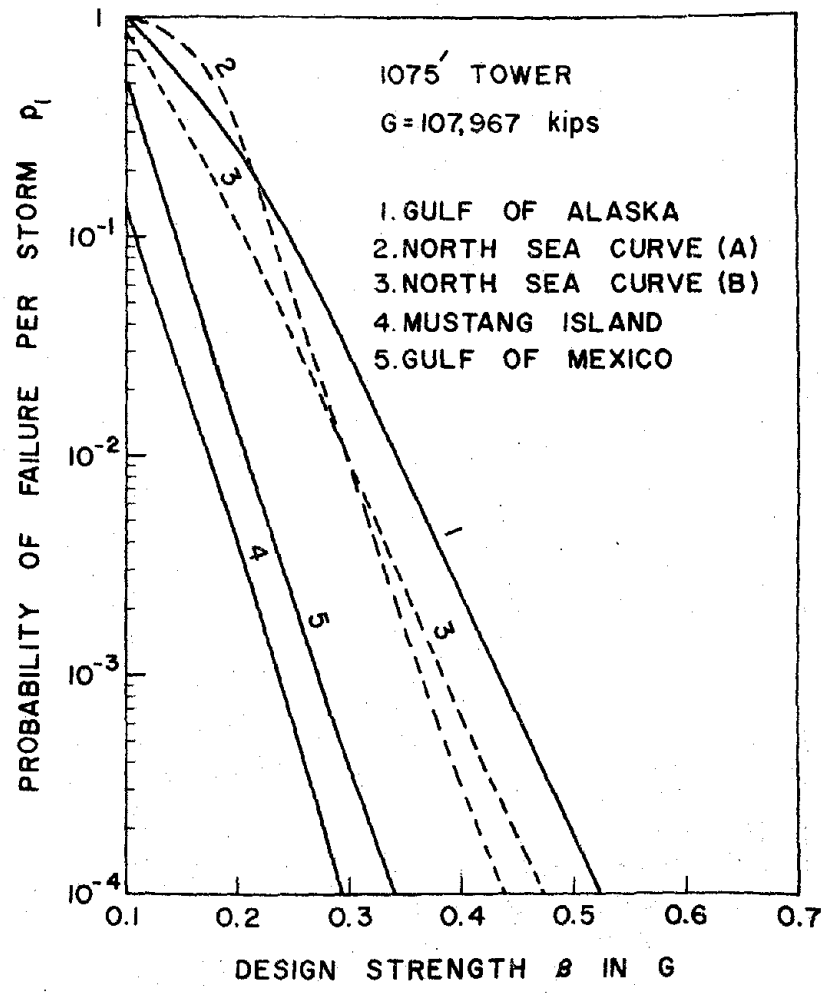

Fig. 16(a): 1075' Tower

Fig. 16: Probabilities of failure per Storm waves, P_1, vs. the design strength β at various geological locations; (a) 1075' tower, (b) 675' tower, (c) 475' tower.

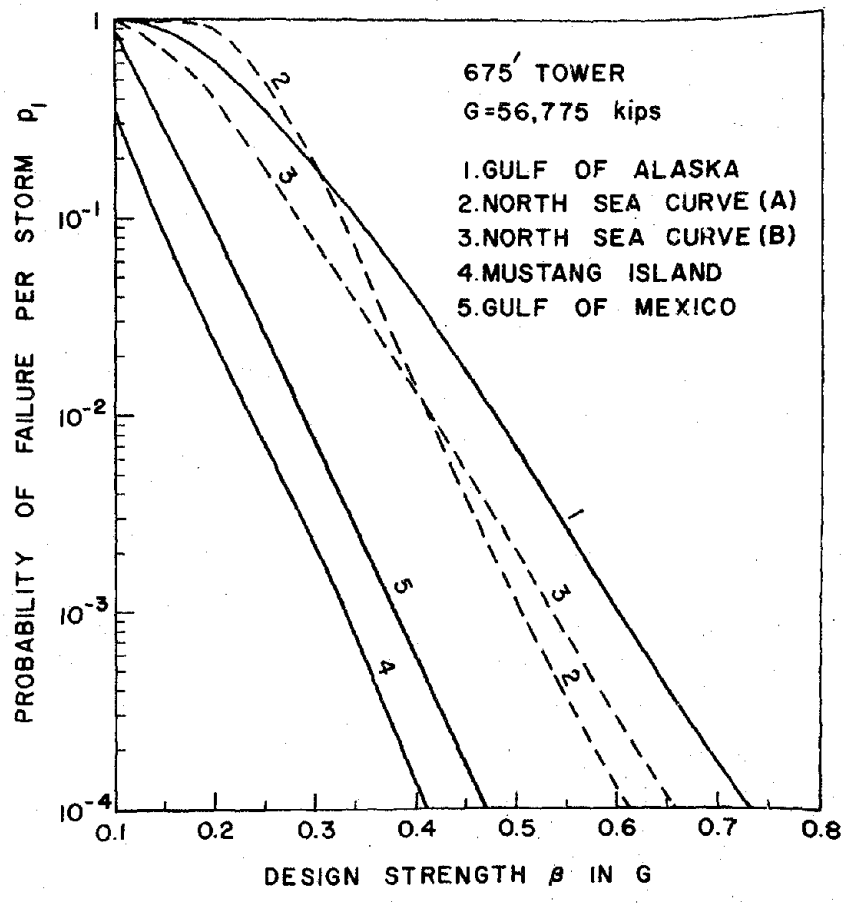

Fig. 16(b): 675' Tower

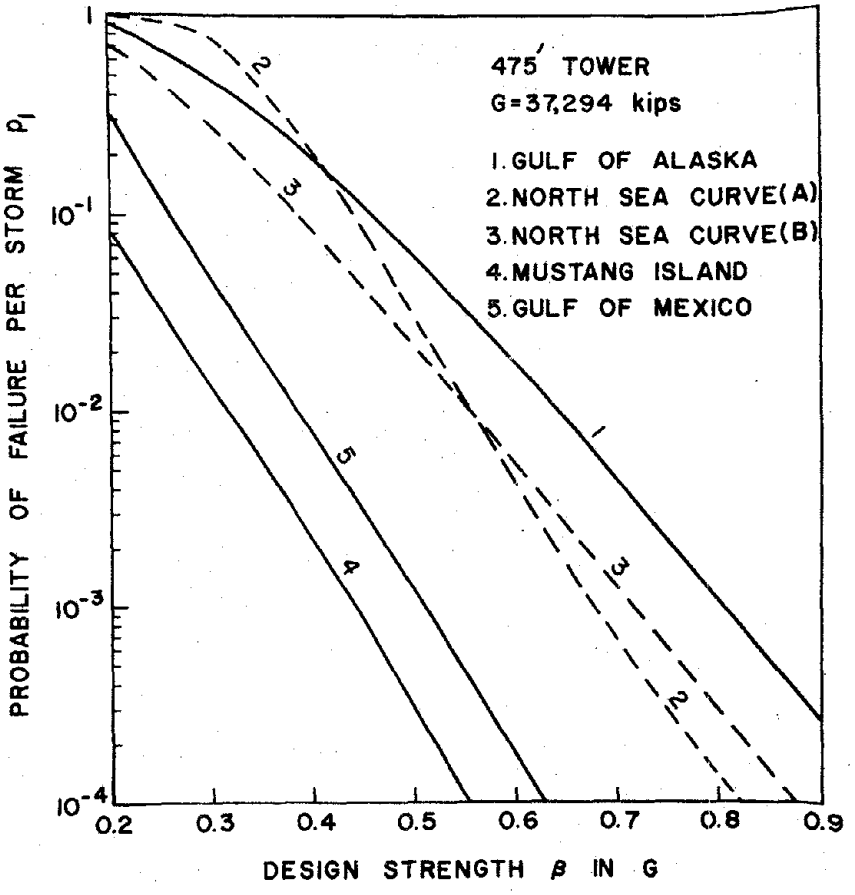

Fig. 16(c): 475' Tower

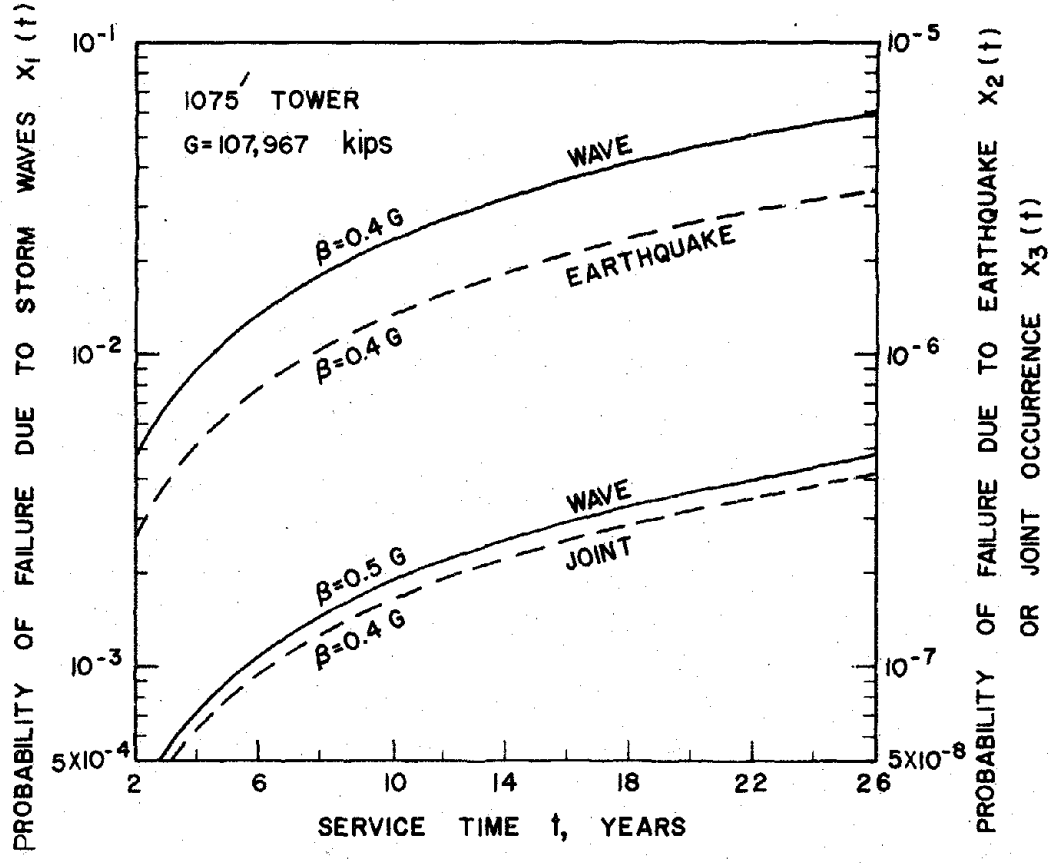

Fig. 17(a): 1075' Tower

Fig. 17: Probabilities of failure vs. service time t in the Gulf of Alaska; (a) 1075' tower, (b) 475' tower.

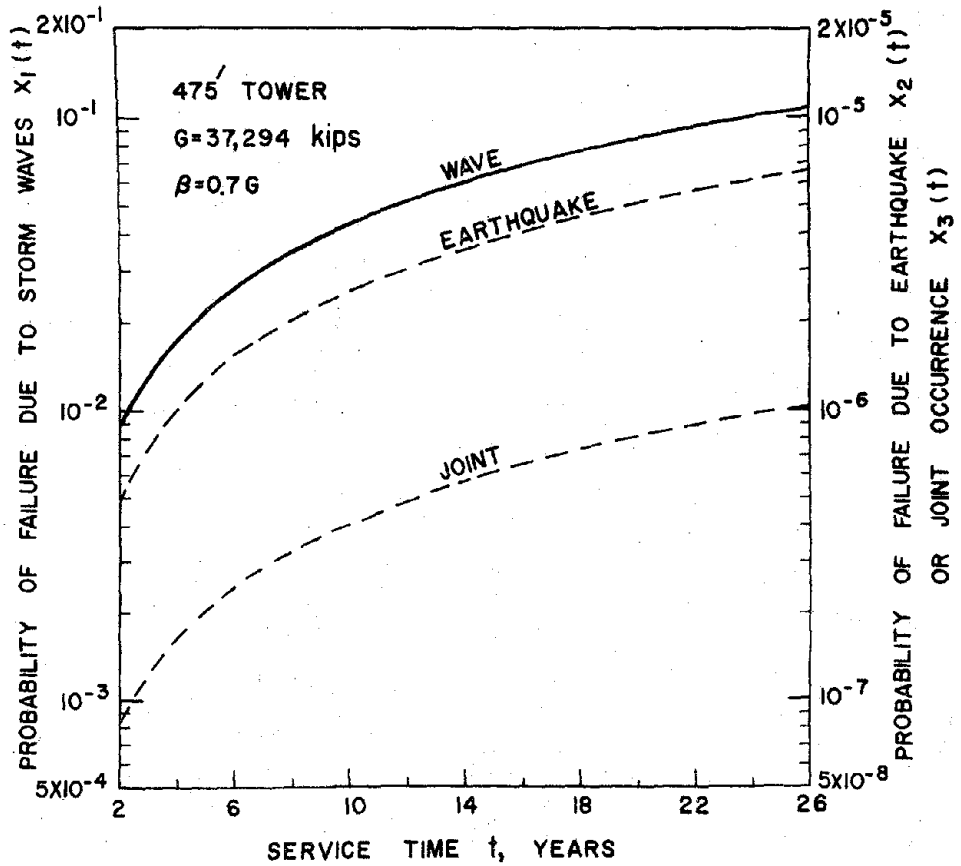

Fig. 17(b): 475' Tower

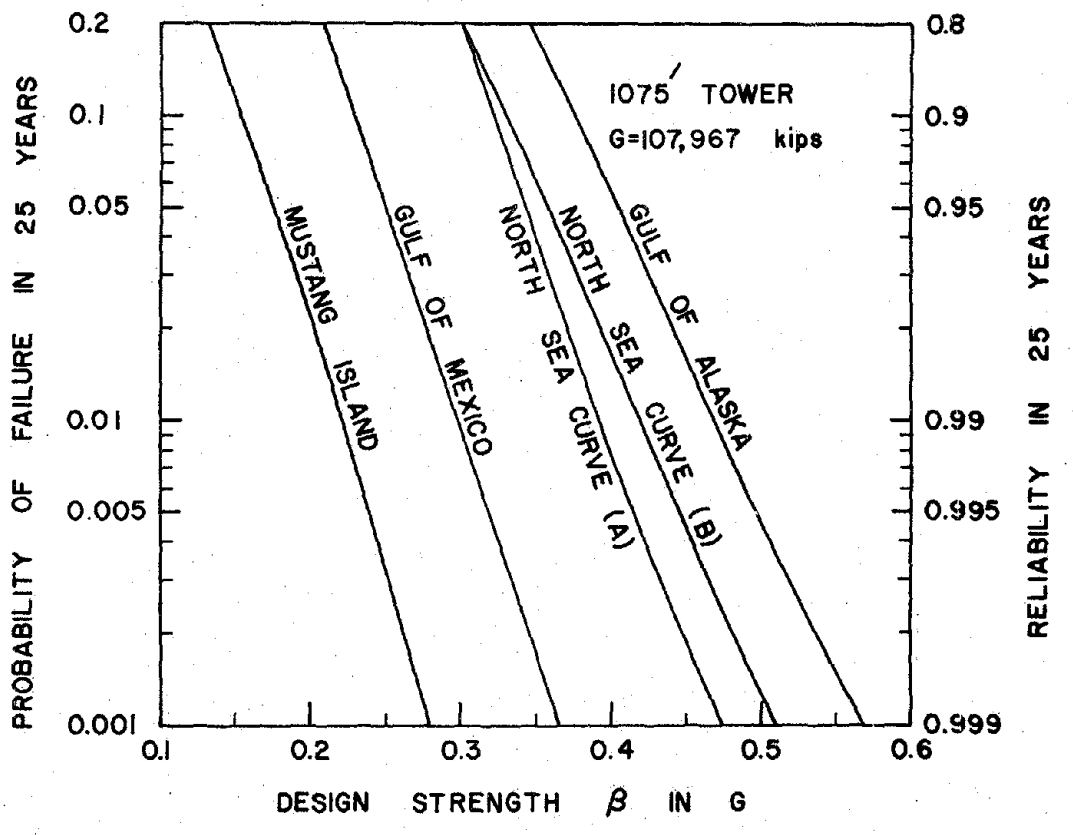

Fig. 18(a): 1075' Tower

Fig. 18: Probabilities of failure (and reliability) in 25 years of service vs. design strength β; (a) 1075' tower, (b) 675' tower, (c) 475' tower.

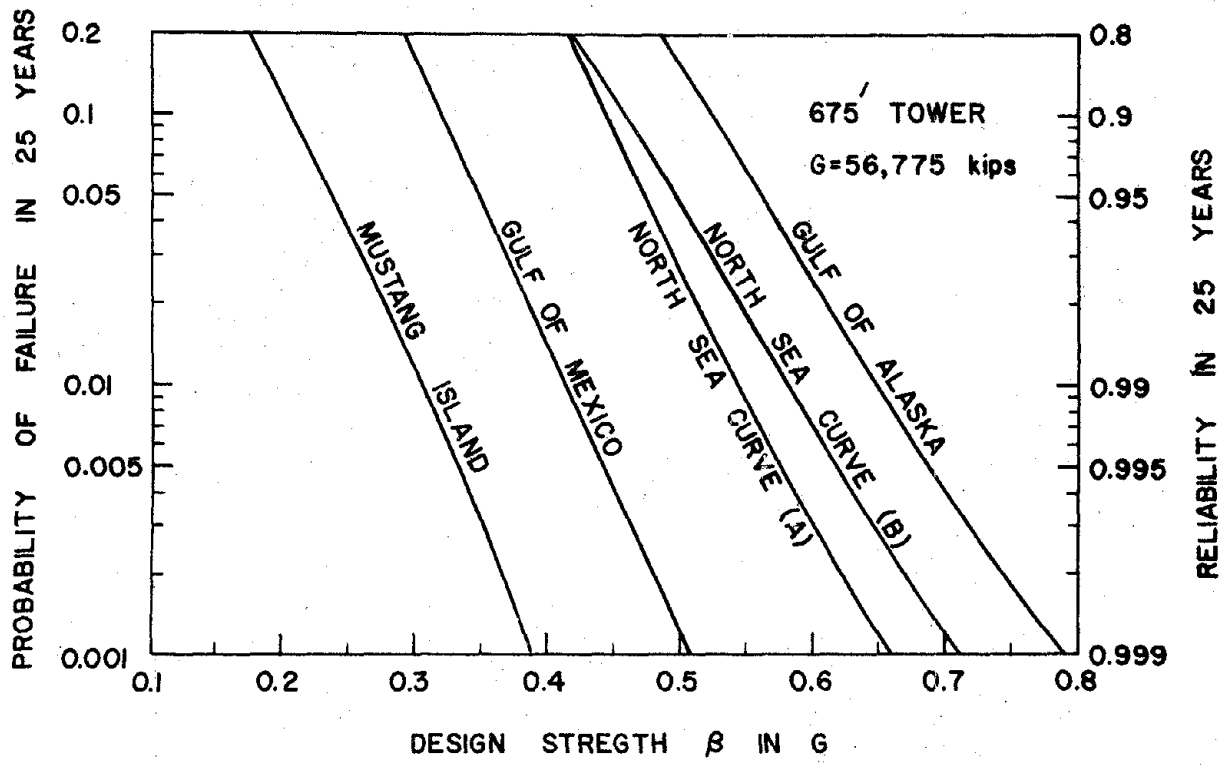

Fig. 18(b): 675' Tower

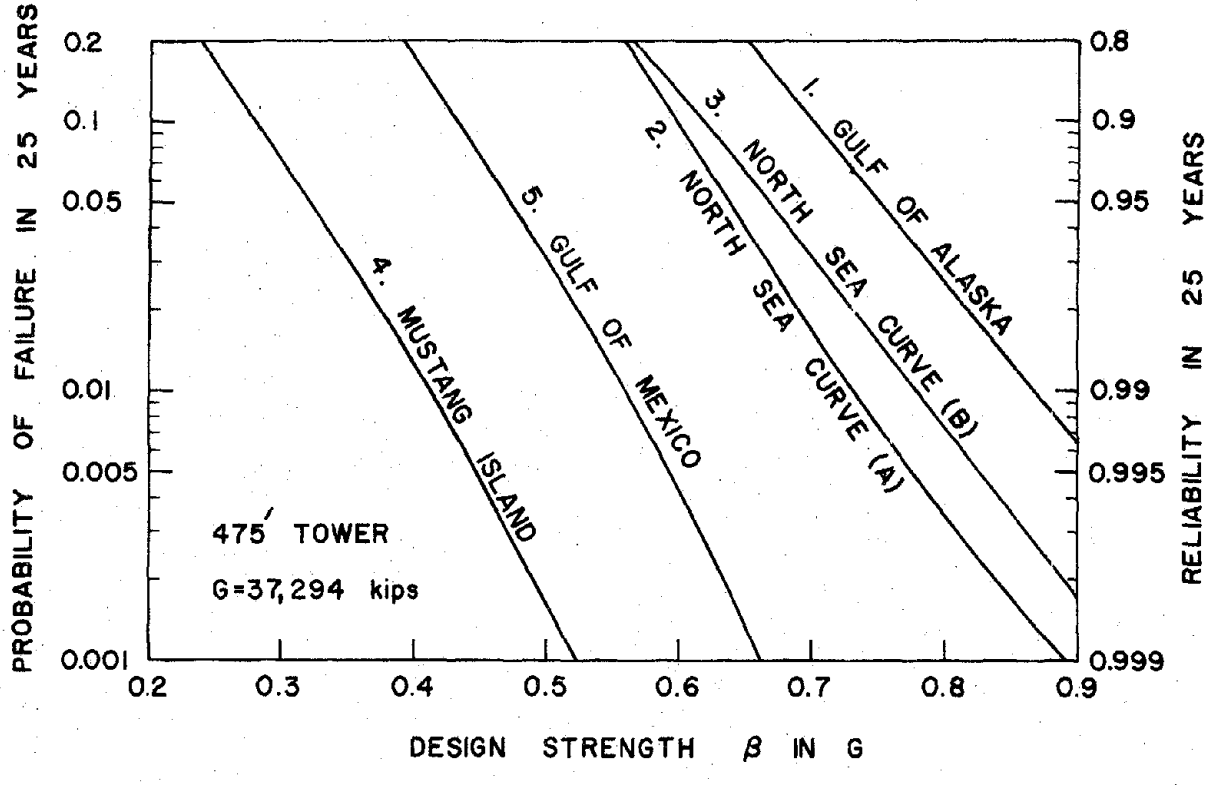

Fig. 18(c): 475' Tower